Site-Directed Mutagenesis Studies of Conserved Metal-Binding Residues in DmpFG, a Bifunctional Aldolase/Dehydrogenase from *Pseudomonas sp.* Strain CF600

Andrew Tait

A Thesis

in

The Department

of

Chemistry & Biochemistry

Presented in Partial Fulfillment of the Requirements

For the Degree of Master of Science at

Concordia University

Montreal, Quebec, Canada

September 2004

Your file Votre référence
ISBN: 0-612-94670-3
Our file Notre référence
ISBN: 0-612-94670-3

ABSTRACT

Site-Directed Mutagenesis Studies of Conserved Metal-Binding Residues in DmpFG, a Bifunctional Aldolase/Dehydrogenase from *Pseudomonas* sp. Strain CF600

Andrew Tait

DmpFG is bifunctional aldolase/dehydrogenase which catalyzes the last two steps of the *meta*-cleavage pathway of catechol in *Pseudomonas* sp. strain CF600. 4-Hydroxy-2-ketovalerate undergoes divalent cation-dependent aldol cleavage to yield pyruvate and acetaldehyde, and the acetaldehyde is then oxidized to acetyl-CoA in an NAD^+- and CoA- dependent reaction. Because of its unique primary sequence, structure, and requirement for Mn^{2+}, DmpG (aldolase) apparently represents a new sub-class of class II aldolases. X-ray crystallography of DmpFG identified His200 and His202 of a conserved HXH motif in DmpG as potential active-site residues; these histidines were observed to be complexed with a metal ion, which in turn was complexed with a molecule of substrate-analogue (Manjasetty, B. A., Powlowski, J., Vrielink, A. (2003) *Proc. Natl. Acad. Sci.* 100(12) 6992-6997).

To evaluate the structural and functional importance of His200 and His202 of DmpG, H200A, H202A, H203A and H202AH203A variants were constructed, expressed and purified. Characterization of the isolated DmpFG proteins indicated that all variants were primarily tetrameric and folded similarly to wild-type enzyme. Differences in fluorescence emission spectra suggested that tertiary structures of the variants were altered. Steady state kinetic analysis of the variants showed that while the apparent k_{cat} was not very different compared to wild-type enzyme, the K_M for 4-hydroxy-2-ketvalerate was increased by more than several-fold for the H200A, H202A and

H202AH203A variants. IC50 values for oxalate, an inhibitor, were also similarly increased. An investigation of the enzymes' metal-ion requirements for activity showed that Co^{2+} can stimulate activity the same as, or better than, Mn^{2+}, which was the only metal ion activator known previous to this work. ICP-MS metal analysis showed that WT and H203A enzymes were isolated with ≈ 1 eq. of metal-ion per subunit of DmpG, while the other variants had substantially lower quantities of bound metal ions. Urea-induced denaturation studies indicated that wild-type > H200A > H202A for stability, correlating with the amount of metal ion bound. Taken together, these observations suggest that His200 and His202 are important for efficient substrate binding and metal ion selectivity, but are not essential for catalysis. Also, His203 does not appear to substitute for His202.

ACKNOWLEDGEMENTS

First and foremost, I thank Dr. Justin Powlowski for his unending support; his guidance as M.Sc. supervisor has helped strengthen my independence not only as a researcher but as an individual.

My sincere gratitude goes out to Dr. M. J. Kornblatt, whom I owe special credit for giving me a start in research and for fostering my curiosity in science.

Appreciation goes to Dr. Joanne Turnbull for good conversation, for allowing me to sound off about whatever was on my mind, especially the results that were leaving me at wit's end.

A big thanks to my lab mates, Dr. Lena Sahlman, Yu Lei, Amy Wong and Jun Man, whose bright spirits and willingness to help each other out made working in the lab a pleasure.

Thanks to Dave Yeung for his help with WebLab.

A VERY SPECIAL THANKS TO:
Mom and Dad, who gave all they had so that I could succeed.
Natalie, whose boundless love has been my driving force to be a better man.
the Carruthers, for their much appreciated support, financial and otherwise.
…and God, for His blessings and making one heck of a good puzzle.

TABLE OF CONTENTS

RESULTS

LIST OF FIGURES

LIST OF TABLES

LIST OF ABBREVIATIONS

4H2KV, 4-hydroxy-2-ketovalerate

α-IPM, α-isopropylmalate

AUC, analytical ultracentrifugation

BCA, bicinchoninic acid

BSA, bovine serum albumin

CD, circular dichroism

CoA, coenzymeA

Dmp, dimethylphenol

DTT, dithiothreitol

E. coli, *Escherichia coli*

EDTA, ethylenediaminetetraacetic acid

Gd·HCl, guanidine hydrochloride

HEPES, 4-(2-hydroxyethyl)-1-piperazineethanesulfonic acid

HMG-CoA, 3-hydroxy-3-methylglutaryl-CoA

IPTG, isopropyl-1-thio-β-D-galactopyranoside

ICP-MS, inductively coupled plasma mass spectrometry

NAD^+, nicotinamide dinucleotide, oxidized

NADH, nicotinamide dinucleotide, reduced

PAGE, polyacrylamide gel electrophoresis

PD, 50 mM Na^+-K^+ phosphate, pH 7.4, with 1 mM DTT

SDS, Sodium dodecyl sulfate

TCA, tricholoacetic acid

TCEP, Tris(2-carboxyethyl)phosphine

Tris, Tris[hydroxymethyl]aminomethane

UV, ultraviolet

WT, wild type

INTRODUCTION

Phenol, also known as hydroxybenzene or carbolic acid, is a stable aromatic compound currently used in many industrial processes. It is mass produced for the manufacture of such commodities as resins, dyes, explosives, insecticides, herbicides and pharmaceuticals. As an historical achievement, Joseph Lister demonstrated that phenol could be used as an antiseptic in surgical techniques, and thus helped establish the importance of sterile methods in medicine (1). Despite its beneficial uses as an antiseptic, phenol also has a reputation for its toxicity to mammals, including its brief use as an orally administered suicide agent (2). Inflicting damage on exposed tissue, phenol can cause irritation and burning of the skin and GI tract, and has detrimental effects on the immune and nervous systems (3). Because billions of kilograms of phenol are produced world-wide annually, degradation of phenol and its derivatives is of obvious interest.

Persistence of phenol in the environment is generally not problematic, as indigenous bacteria in soil and water can efficiently metabolize it at appreciable rates (4). Phenols with multiple ring substituents are unfortunately more recalcitrant to natural degradation, so therefore the study of many bacterial species which have different tolerances to these compounds, and understanding the diversity of catalytic mechanisms, would be of interest. Directed evolution studies on bacterial pathway enzymes will hopefully allow for more efficient catalysis and degradation of a wider range of phenol-based compounds.

Phenol degradation by bacterial organisms

Reports of microbes capable of metabolizing phenol began to emerge in the 1920's and 30's (5, 6). An explosion of biochemical studies done in the 60's and 70's helped to characterize the *meta*-cleavage pathway of phenol degradation (Figure 1), whereby phenol is first hydroxylated to catechol and then aromatic ring-cleavage occurs adjacent to two hydroxyl groups (7). Certain bacteria can also use the *ortho*-cleavage pathway, catalyzing ring fission between the two catechol hydroxyls (8). Both *ortho* and *meta* pathways employ different pathway enzymes, and also have different tolerances and efficiencies for metabolizing phenols and phenols with various ring substituents.

One very efficient phenol degrading organism that has been isolated (9) and well-studied (10) is *Pseudomonas* sp. strain CF600, a bacterium which utilizes the *meta*-cleavage pathway. The fifteen genes for the entire phenol degradation pathway are grouped together in an operon approximately 15 kb in length, encoded on a large plasmid, pVI150, which exceeds 200 kb in size (Figure 1). Nine enzymes are involved in the phenol catabolic pathway in *Pseudomonas* sp. strain CF600. Transcription of the pathway enzymes is controlled by DmpR, a σ^{54}-dependent transcription regulator that effects gene expression in response to phenol compounds, so that the pathway enzymes are expressed only when substrates are present (10). Phenol hydroxylase, a multi-component enzyme separate from the pathway, primes phenol for ring cleavage at the *meta*-position by adding a hydroxyl

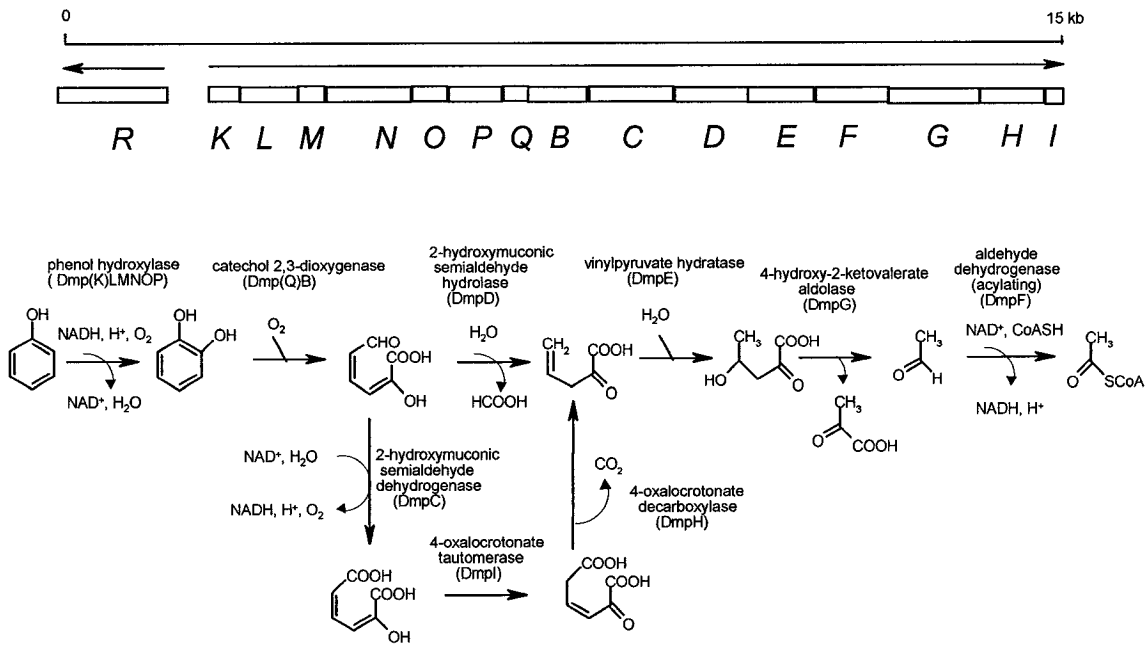

Figure 1: The *meta*-cleavage pathway and associated phenol hydroxylase from *Pseudomonas* sp. strain CF600. Genes for the pathway are encoded in a 15 kb region on the 200 kb pVI150 megaplasmid, and denoted at the top. The pathway intermediates and the different enzymes involved in catalysis are illustrated on the bottom half of the figure. Figure is adapted from (10).

group to phenol, creating catechol (10), and oxygenative ring opening is then catalyzed by catechol-2,3-dioxygenase, or DmpB, the first enzyme of the *meta*-cleavage pathway. As illustrated in Figure 1, the subsequent *dmp*-encoded pathway enzymes catalyze a series of reactions to yield pyruvate and acetyl-CoA as final products. These product molecules can then enter the Krebs cycle and glycolytic pathways. This allows the organism to grow using phenol as a sole source of carbon and energy.

4-Hydroxy-2-ketovalerate aldolase (DmpG) and aldehyde dehydrogenase (acylating) (DmpF) complete the *meta*-cleavage pathway

At the end of the *meta*-cleavage pathway is the bifunctional enzyme complex, 4-hydroxy-2-ketovalerate aldolase (DmpG) / acetaldehyde dehydrogenase, acylating (DmpF), which catalyses the conversion of 4-hydroxy-2-ketovalerate to pyruvate and acetyl-CoA (Figure 1). The molecular masses of DmpF and DmpG are 32.5 kDa and 37.5 kDa, respectively, and two polypeptides of each are tightly associated in a tetramer, forming a 140 kDa active complex (11, 12). Structural (13) and enzyme kinetic data (14) provide evidence suggesting that substrate channeling occurs between the two subunits. As revealed by X-ray crystallography, the subunits are arranged in a semi-linear fashion, with two subunits of DmpG associated in the middle and two subunits of DmpF at the periphery (Figure 2). The term 'DmpFG' will refer to the tetrameric form of the enzyme complex for the remainder of this thesis.

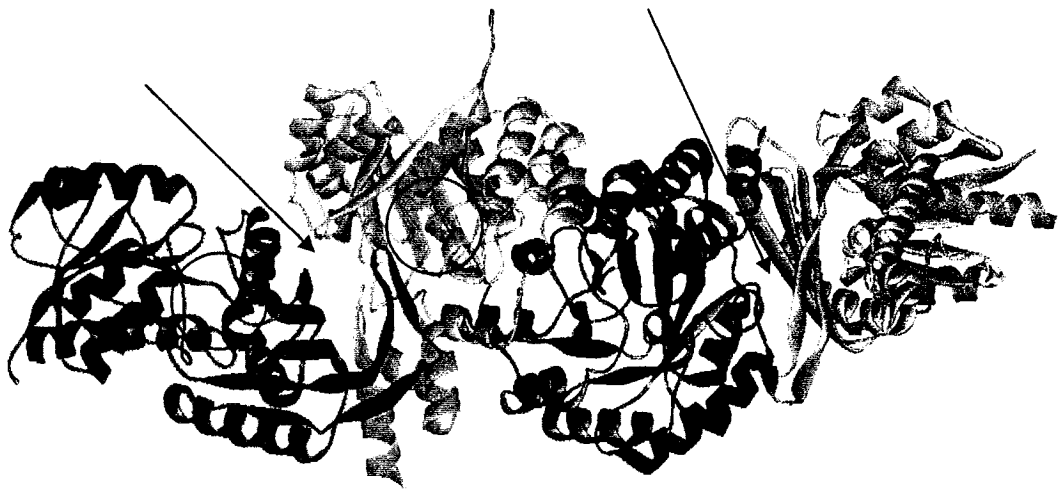

Figure 2: Structure of DmpFG from *Pseudomonas* sp. strain CF600. The two central DmpG subunits are in varying shades of green; the two DmpF subunits, seen at the peripheral ends of the molecule, are in shades of pink. Arrows indicate the proposed tunnel regions between the DmpF and DmpG subunits, and active site locations are circled for one of each type of subunit. PDB coordinates are 1NVM (15).

Structure of DmpF: a dehydrogenase resembling glyceraldehydes-3-phosphate dehydrogenase

DmpF represents a novel primary sequence for a dehydrogenase, but the overall structure resembles that of the glyceraldehyde-3-phosphate dehydrogenase family (13). There are two domains of DmpF: an N-terminal NAD^+ binding domain (residues 1-130) and C-terminal dimerization domain (residues 286-312). In the crystal structure, both holo and apo forms of DmpF are observed, i.e.: with (holo) and without (apo) NAD^+ bound. Certain conformational differences exist between the two forms, most notably the positioning of Cys132, the only conserved cysteine residue among the aldehyde dehydrogenase (acylating) family. In the apo form, water is bound between Cys132 and adjacent Asp209, but in the holo form, the water is absent and the side chain thiol of cysteine can move to face the nicotinamide ring of NAD^+. Consistent with a role for Cys132 in catalysis, a thiol-modifying reagent, iodoacetate, abolishes the dehydrogenase activity (14). Also, the presence of NAD^+ in DmpF causes distinct conformational changes within the DmpG subunit, which may be important for promoting substrate channeling (15).

Structure of DmpG: a new metal-dependent (class II) aldolase

DmpG is comprised of two domains, an N-terminal $(\alpha/\beta)_8$ TIM barrel (residues 1-250), and a C-terminal communication domain (residues 251-345) that interacts with the DmpF subunit. DmpG is stimulated by divalent metal ions, 6-8 fold upon addition of Mn^{2+} (11),

and is thus established as a class II aldolase. Class II aldolases are enzymes found primarily in bacteria, fungi, yeast, and blue-green algae (16). Unlike their class I counterparts that are found in higher organisms and require Schiff-base formation at a lysine residue for catalysis, class II aldolases require metal ions for enzymatic activity. The role of this metal ion is as a Lewis acid, thereby polarizing the carbonyl bond of incoming substrates to promote adjacent carbon-carbon bond cleavage and proton transfer to subsequent enolate intermediate (17). This reaction mechanism is consistent with all class II aldolases, although the catalytic residues involved may differ.

Structures have been reported for five different Class II aldolases: L-fuculose-1-phosphate aldolase (18), L-rhamnulose-1-phosphate aldolase (19), 2-dehydro-3-deoxygalactarate aldolase (20), fructose-1,6-bisphosphate aldolase (21) and tagatose-1,6-bisphosphate aldolase (22). Class II aldolases can be categorized as those that have an $(\alpha/\beta)_8$ TIM barrel fold (2-dehydro-3-deoxygalactarate aldolase, fructose-1,6-bisphosphate aldolase and tagatose-1,6-bisphosphate aldolase) and those that do not (L-fuculose-1-phosphate aldolase, L-rhamnulose-1-phosphate aldolase). Fructose fructose-1,6-bisphosphate aldolase and tagatose-1,6-bisphosphate aldolase can be grouped together into one subclass of the $(\alpha/\beta)_8$ TIM barrel class II aldolases on the basis of their sequence similarity and preference for binding Zn^{2+}, whereas 2-dehydro-3-deoxygalactarate aldolase forms another subclass on the basis of its unique sequence and dependence on Mg^{2+}. The lack of sequence identity between DmpG and any of the known $(\alpha/\beta)_8$ TIM barrel class II aldolases suggests that DmpG represents a third subclass (15).

A BLAST database (23) search using the DmpG primary sequence indicates that DmpG is most similar to the family of 3-hydroxy-3-methyl-CoA (HMG-CoA) lyases (EC 4.1.3.4), exhibiting a 17 % sequence identity with the human form. Unfortunately no crystal structure has been determined for any HMG-CoA lyase. However, functional studies performed in conjunction with site-directed mutagenesis indicate that HMG-CoA lyase and DmpG may share similar active site residues (24). DmpG shows a 15 % sequence identity with α-isopropylmalate (α-IPM) synthase from *M. tuberculosis,* for which a crystal structure was recently solved (25). The two share a similar $(\alpha/\beta)_8$ TIM barrel structure, and have a high identity of proposed active-site residues.

At the active site of DmpG (Figure 3), as seen in the crystal structure (15), there is a metal ion within the $(\alpha/\beta)_8$ TIM barrel, in the-N-terminal barrel domain. The identity of the metal ion is still unclear, but the observed atomic density has putatively been assigned as Mn^{2+}, based on activity and preliminary inductively coupled plasma mass spectrometry data (15). Three metal ligands supplied by the protein are Asp18, His200 and His202 and there is also a water molecule in close proximity (15). The crystal structure also reveals another molecule present, the identity of which is unknown, which donates two carboxyl oxygens as metal ion ligands. The electron density of this molecule in consistent with both pyruvate, the product, and oxalate, a structural analog of pyruvate. The origin of this molecule is not clear at present.

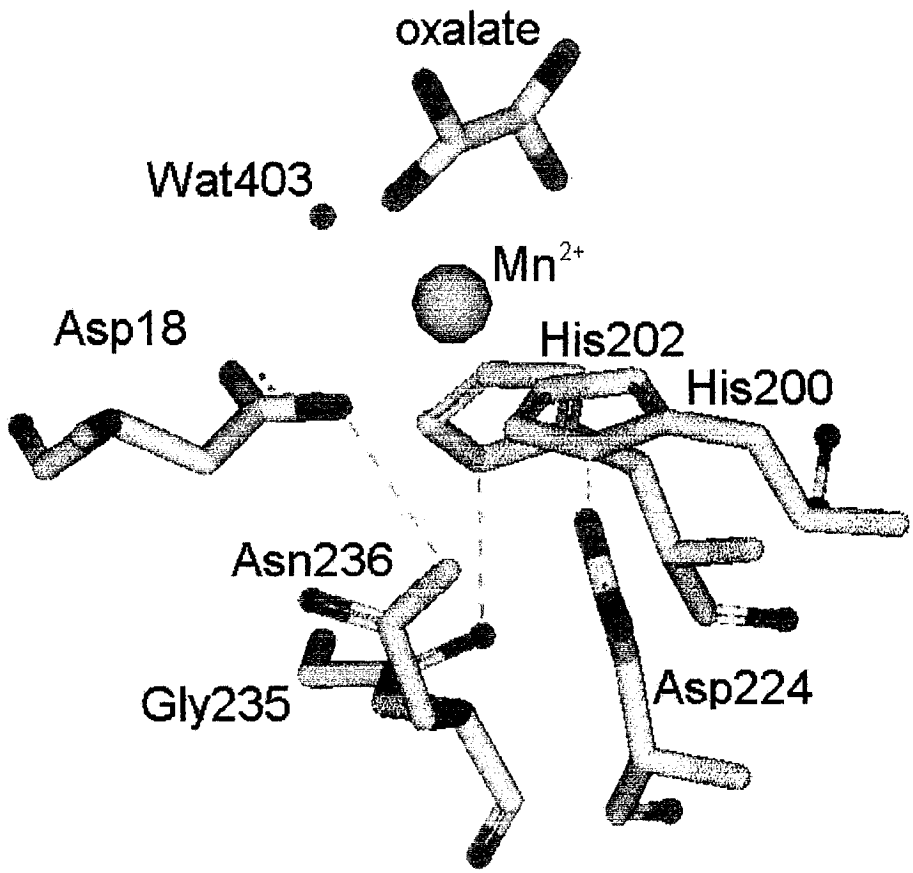

Figure 3: Side-chain stabilization of metal ion ligands by hydrogen bonding with surrounding residues in DmpG. Hydrogen bonding is denoted by green dotted lines. Asp18 hydrogen bonds with Asn236 Nδ2, His200 with Asp224 Oδ1, and His202 with the side-chain carbonyl oxygen of Gly235. Model was based on PDB file 1NVM, constructed using WebLab Viewer software (Accelrys).

Channeling of a toxic intermediate between DmpF and DmpG?

Acetaldehyde is proposed to be channeled directly from DmpG to DmpF between the two subunits (Figure 2). The function of substrate channeling in DmpFG may be vitally important in preventing, or at least minimizing, the organism's exposure to toxic acetaldehyde, which is produced together with pyruvate when 4-hydroxy-2-ketovalerate undergoes DmpG-catalyzed aldol cleavage (Figure 3). Structural evidence shows that a 29 Å-long tunnel stretches between the DmpF and DmpG active sites (13, 15). The role of Tyr291 of DmpG has been proposed to gate entry to the tunnel, and prevent acetaldehyde from leaking back out once it has entered (15). Hydrophobic DmpF residues Ile-172, Ile196 and Met-198 block the end of the putative tunnel, gating access to the active site of DmpF, where NAD^+ is used to oxidize acetaldehyde and CoA is added to form acetyl-CoA.

Earlier analyses revealed that DmpG is mainly insoluble (14) unless co-expressed with DmpF and consequently there is no detectable aldolase activity in the absence of DmpF (12). One interpretation of such data is that DmpF must be present not only to maintain solubility and consequent functionality of DmpG, but also accept the acetaldehyde as it is produced without allowing it to leak into the bulk solvent. Preliminary kinetic evidence further supports the idea of a channeling mechanism as the K_M for exogenous acetaldehyde exceeds 50 mM, a physiologically irrelevant concentration for such a toxic compound (J. Powlowski, unpublished data). This suggests that acetaldehyde has difficulty accessing the DmpF active-site unless the compound is directly channeled from the DmpG active-site. To directly test the hypothesis of channeling, future studies will involve site directed

mutagenesis to block the channel, thereby allowing the acetaldehyde to leak out, and seeing if this leakage causes problems for viability.

Comparison of DmpG and α-IPM synthase active site structures

The study of α-IPM synthase has been limited to only a few organisms. The enzyme has been shown to exist in either dimeric (*S. cerevisiae*) (26) or tetrameric (*S. typhimurium*) (27) forms, and exhibits a divalent metal ion requirement. In α-IPM synthase, an acetyl group is removed from acetyl-CoA and added to a molecule of α-ketoisovalerate to give α-IPM at the start of the leucine biosynthesis pathway. Despite having only 15% sequence identity, DmpG and α-IPM synthases fold into similar $(\alpha/\beta)_8$ TIM barrel structures. The structure of the dimeric α-IPM synthase of *M. tuberculosis* is much like the DmpG dimer at the center of the DmpFG tetramer (25, Figure 5A). Thus a comparison of the structures of DmpG and α-IPM synthase (*M. tuberculosis*) can provide insight into possible roles of active site residues. Despite similar active site arrangements, proposed catalytic mechanisms of both enzymes are somewhat different. While DmpG catalyzes aldol cleavage, α-IPM synthase catalyzes the reverse type of reaction, an aldol condensation (25). The role of the divalent metal ion in α-IPM synthase is proposed to be similar to DmpG insofar as the metal enables polarization of the substrate carbonyls. However, instead of breaking the carbon-carbon bond adjacent the polarized carbonyl, the carbonyl is primed for nucleophilic attack by the incoming acetyl group of acetyl-CoA, which bares a carbanion subsequent to proton abstraction from the acetyl methyl group.

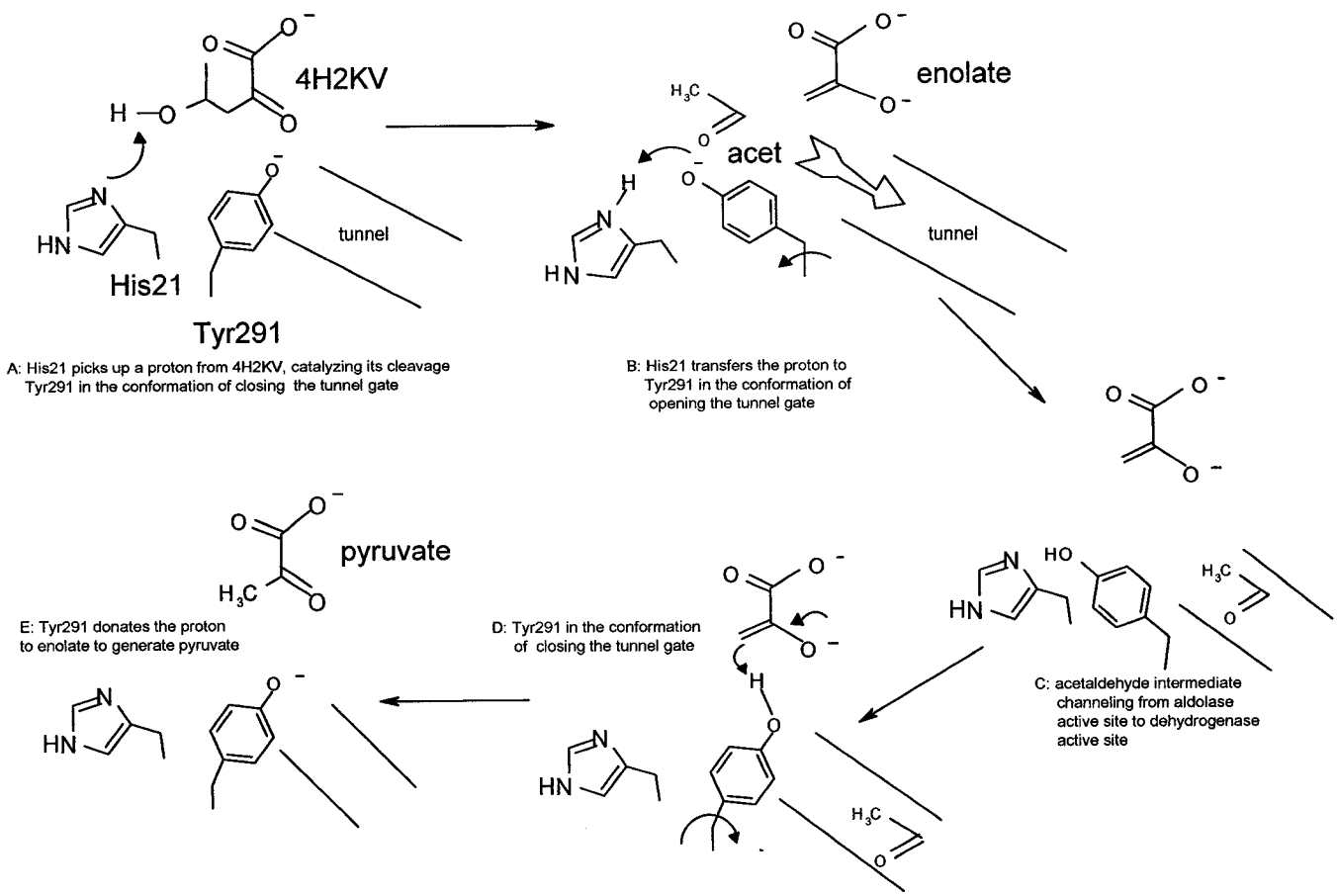

Figure 4: Proposed mechanism of DmpG catalysis and access to tunnel leading to DmpF active site. The substrate binds at the active site of DmpG, polarized by the bound divalent metal ion, Mn^{2+} (not shown) to permit aldol cleavage. Figure was adapted from (15) and was graciously provided by and reproduced with permission from Yu Lei.

Virtually all active site and surrounding amino acids are conserved or are at least similar in DmpG and α-IPM synthase (Figure 6). Metal ligand residues Asp18, His200 and His202 of DmpG correspond to Asp81, His285 and His285 of α-IPM synthase. Likewise, His21 and Tyr291, proposed catalytic residues of DmpG, are equivalent to His379 and Tyr410. Interestingly, in α-IPM synthase these two residues and the rest of the corresponding active-site residues are not on the same subunit, but are brought into proximity of the substrate by a domain-swapping arrangement of both subunits (25). In DmpG, Arg17 and Ser171 are suggested to hydrogen bond with the substrate, as are α-IPM synthase's Arg80 and Thr254, respectively. In both enzymes, the positively-charged side chains of the aforementioned arginines are well-positioned to stabilize the enolate intermediate once it is formed. One key difference between the active sites is the identity of the residue proposed to be involved in proton abstraction from the substrate. In α-IPM synthase, both Glu218 and His379 are in positions close enough to allow them to catalyze proton abstraction, but in DmpG there is less ambiguity since only His21 appears to be in close enough proximity to the substrate to catalyze proton removal.

Koon *et al.* (25) observed that similarities between α-IPM synthase and DmpG extend beyond the proposed principal active-site residues. Just outside the sphere of the active site, certain residues act via hydrogen bonding to rigidly hold in place the amino acid side chains that ligate the divalent metal ion (Figure 4). Side-by-side glycine and asparagine residues are invariant (Gly235 and Asn236 in DmpG and Gly320 and Asn321 in α-IPM synthase); where DmpG has an aspartic acid (Asp224), there is a glutamic acid in α-IPM

A

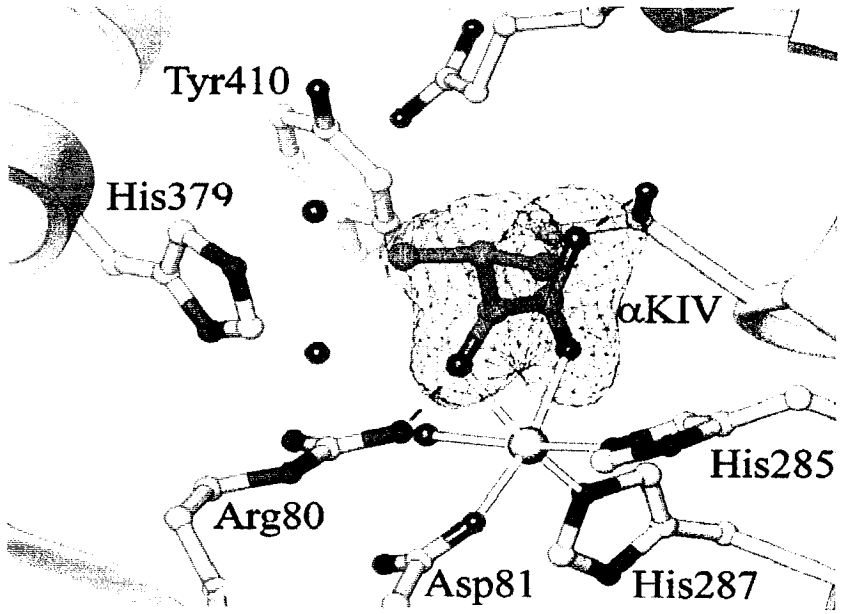

B

Figure 5: Active-site representations of A) α-ketoisovalerate synthase from *M. tuberculosis* and B) HMG-CoA lyase from *H. sapiens*. In A), ligands to the Zn^{2+} ion (magenta) are illustrated by tubes and hydrogen bonding between Arg80 and carbonyl oxygen of the α-ketoisovalerate (α-KIV) substrate is designated by a dotted line. B) represents a potential active site arrangement of human HMG-CoA lyase, modeled after the structure of DmpG. A) and B) are adapted from (25) and (24), respectively.

HOA *P. sp.* strain CF600 (P51016)	16-LRDG	199-MHAHH	223-VDASLAGMGAGAGNA
HOA *P. putida* (P510157)	15-LRDG	198-MHAHH	222-IDGSVAGLGAGAGNT
HOA *B. cepacia* (P51015)	15-LRDG	198-FHGHH	222-IDAAAAGLGAGAGNT
IMS *S. cerevisiae* (P06208)	68-LRDG	274-THCHN	298-VEGCLFGNGERTGNV
IMS *H. influenzae* (P43861)	12-LRDG	200-VHCHN	225-IEGTINGIGERAGNT
IMS *M. tuberculosis* (CAA18032)	79-LRDG	286-LHPHN	308-IEGCLFGNGERTGNV
HMGL *H. sapiens* (P35914)	40-PRDG	232-VHCHD	256-VDSSVAGLGGCPYAK
HMGL *P. mevalonii* (P13703)	11-PRDG	203-GHFHD	227-FDSSVAGLGGCPYSP
HMGL *C. eligans* (AAK73908)	26-ARDG	219-VHFHD	243-ADSSIAGLGGCPYAK

Figure 6: Illustration of selected conserved active-site residues in 4-hydroxy-2-ketovalerate aldolase (HOA), α-isopropylmalate synthase (IMS) and 3-hydroxy-methylglutaryl lyase (HMGL) from various species. Enzyme name abbreviation is followed by the organism name and the corresponding accession number. The first and second columns are the metal-binding residues observed in x-ray crystal structures of HOA or DmpG (15) and IMS (25), and the third column represents the residues that stabilize the metal ligands via hydrogen-bonding.

synthase (Glu309) to serve a similar function. Such an arrangement may be necessary to not only allow tight metal binding of the enzyme, but also maintain the necessary active site environment that is optimal for the substrate binding and specificity. Furthermore, hydrogen bonding in these cases undoubtedly contributes to the global stability of the protein.

HMG-CoA lyase: possible insights into DmpG catalysis

HMG-CoA lyase is involved in leucine catabolism of many organisms, and catalyzes the cleavage of HMG-CoA into acetyl-CoA and acetoacetate (28). Like DmpG, the enzyme has a requirement for divalent metal ions for activation (29). Mn^{2+} or Mg^{2+} can act as dissociable activators metal ions and the affinity for each is quite different; K_M for Mn^{2+} in the human enzyme is 0.34 μM, 3 orders of magnitude lower than for Mg^{2+} whose K_M is 233 μM. The K_M for the HMG-CoA substrate is 50 μM. Human disease associated with mutations within the enzyme (30) has guided the construction of recombinant variants for functional analysis. With many of the variant HMG-CoA lyases characterized in terms of substrate and metal ion affinity and overall catalytic efficiency (31, 32, 24, 33, 29), we may be able to predict how similar variants of DmpG would behave.

The structure of HMG-CoA lyase has not been solved, but modeling of the human variant has been done independently by two different groups, with the models based on the α/β barrel templates of DmpG (24), and phosphoribosylformamino-5-aminoimidazole carboxamide ribonucleotide (PFAR) isomerase (34). DmpG proves to be a better template

for HMG-CoA lyase because of alignment of key active-site residues and the overall similarity of cleavage reactions that are catalyzed (24). Previous to modeling efforts, several proposed active-site residues of HMG-CoA lyase (Figure 5B) have been identified by site-directed mutagenesis: His233, His235 and Asp42 which are equivalent to DmpG metal ligands His200, His202 and Asp18, respectively. Of these, only His235 (32) and Asp42 (33) have been implicated in metal binding by measuring K_M's and K_D's for activator metals ions of variants as compared to WT. Interestingly, since it is contrary to what might be expected from viewing the structure of DmpG, variants in which His233 is replaced not affect metal binding (31). Glu72, however, (corresponding to DmpG Glu48) is found to be a third protein ligand to the activator metal ion (33). His235, Asp42, and Glu72 are involved not only in cation binding, but also appear to be important for HMG-CoA substrate affinity (32, 33). While mutation of the His233 residue results in a major loss of specific activity, there is no change in affinity for either metal ion or substrate (31). Another identified active-site residue that is essential for catalysis is Arg41 (corresponding to DmpG Arg17), as variants substituted with different amino acids at this position are virtually inactive; the arginine side chain is positioned for hydrogen bonding with a substrate oxygen and also is hypothesized to stabilize an enolate intermediate (24). Cys266 is a residue conserved in HMG-CoA lyases and mutagenesis studies demonstrate that the residue aids in maintaining WT HMG-CoA lyases's high specific activity (29). However, this cysteine residue is absent from families of DmpG and α-IPM synthase (Figure 6). The cysteine residue appears to have replaced the conserved side-by-side glycine-asparagine involved in hydrogen bonding to the metal-ligand of DmpG (Figure 4) and α-IPM synthase, although the third hydrogen bonding residue, an aspartic acid, is

present in HMG-CoA lyase. While substituting for this Cys266 results in significant loss of HMG-CoA specific activity, the exact role of this residue remains unknown.

In addition to possessing similar active site configurations, another interesting observation concerning DmpG, α-IPM synthase and HMG-CoA lyase is that the enzyme activities can be modulated by C-terminal control, although by completely dissimilar mechanisms. Not only is the C-terminal of DmpG (communication domain) in contact with DmpF to maintain the enzyme complex stability and solubility, but NAD^+-binding at DmpF can affect the conformation of DmpG, which is a likely explanation for NAD^+/NADH-stimulated aldolase activity (11, 15). At the C-terminal of human HMG-CoA lyase, Cys323 is needed for stability of activity, as the C323S variant was found to be much less stable than the WT enzyme (35). Bacterial HMG-CoA lyase which is naturally missing this cysteine, is markedly less stable than the human counterpart (57). Quite notably, however, the C323S variant of human HMG-CoA lyase has higher specific activity than WT and is less susceptible to inactivation by oxidiation; regulation of mammalian lyase activity is proposed to be modulated by formation of disulfide-linked homodimers (29). At the C-terminus of α-IPM synthase, there is a binding pocket for leucine, which is the end product of the pathway. Leucine binding inhibits synthase activity, and is thus part of a feedback inhibition mechanism.

Thesis Objectives

The main goal of the studies reported here was to examine the role of conserved aldolase (DmpG) residues His200 and His202 in terms of catalytic activity and structural stability of the DmpFG complex. Studies of human HMG-CoA lyase indicate that homologous residues, His233 and His235, are important for catalytic function. Crystallographic studies of DmpFG indicate that these two histidines ligate a metal ion, which is complexed with a molecule that is structurally homologous to the biological substrate. In order to help define the functional roles of these conserved histidines, H200A and H202A were engineered. The purified proteins were subjected to biophysical and kinetic analyses.

After preliminary kinetic analysis demonstrated a high level of aldolase activity in the DmpFG H202A variant, the question was raised whether or not adjacent His203 could substitute for His202. This notion was the rationale behind constructing the H203A and H202AH203A variants.

Another aim was to devise methods to examine the structural stability of DmpFG in response to chemical and thermal denaturation. The utility of establishing such parameters for examining stability would allow for comparison of DmpFG WT with the variants examined in this report, and others that will be engineered for future study.

The variants studied in this thesis refer to mutations made in the DmpG subunit only. In all instances, the DmpG subunit (WT and variants) was co-expressed with the native DmpF subunit.

MATERIALS AND METHODS

Materials. All materials were reagent grade or of the highest available purity. Oligonucleotide primers were synthesized by BioCorp Inc. (Montreal, Quebec, Canada). Lactate dehydrogenase (hog muscle LDH, E.C. 1.1.1.27), and NAD^+ (Grade I) were from Roche, and CoA (trilithium salt) was from MP Biomedicals. NADH was obtained from Sigma and acetaldehyde was from Aldrich. Restriction enzymes were purchased from Promega, Roche or MBI. CoA and NAD^+ and NADH stock solution concentrations were calculated using ε_{260} = 16,800 $cm^{-1}M^{-1}$, ε_{260} = 18,000 $cm^{-1}M^{-1}$ and ε_{340} = 6220 $cm^{-1}M^{-1}$, respectively (36), after dilution in 50 mM HEPES, pH 8.0, at ambient temperature.

Plasmid construction and site-directed mutagenesis. DNA manipulations were performed using standard protocols (37). A subclone of pVI150, pVI316Δ (8), was digested with *XhoII* to generate a 3757 bp fragment that was subsequently ligated into the *BamHI* site of the pT7.5 expression vector (38); the *dmpFG* coding region was thus inserted downstream from the pT7 promoter, to give construct pT7.5-*dmpFG*. This construct was prepared by Dr. J. Powlowski.

A 1650 bp *EcoRI-NotI* fragment, encoding amino acids E68 of DmpF to I300 of DmpG, was excised. from the pT7.5-*dmpFG* construct and inserted into the same sites of the pCRII vector (Invitrogen) to yield a 5512 bp plasmid, pCRII-*dmpF*. This construct was the starting point for mutagenesis. Variants of DmpG having active-site histidines replaced with alanine were engineered using the Quickchange method (Stratagene) using pCRII-*dmpF* as template together with various mutagenic primers (Table 1), which introduced

new restriction sites by silent mutation, as well as the desired amino acid change. Mutagenized plasmids were then used to transform *E. coli* strain XL2-Blue (Stratagene). Transformants were grown on Luria Bertani (LB)-agar plates containing 20 μg/ml kanamycin, and selected transformants were grown in liquid LB medium with the same concentration of antibiotic. Plasmid DNA was purified using a Wizard© Miniprep Kit (Promega) and checked for the introduction of the silent mutation by cutting with corresponding restriction enzymes (Table 1). Once the silent mutation was verified, plasmid DNA was digested with restriction enzymes to produce short subcloning fragments containing the region of variant DNA (Table 1). The fragments were then ligated into the corresponding restriction sites of the pT7.5-*dmpFG* expression vector; transformants were selected from LB-agar plates containing 100 μg/ml carbenecillin, and then grown in LB liquid medium with the same antibiotic. Plasmid DNA was purified and checked for the presence of the desired mutation silent mutation as before. H200A, H202A and H203A variant DNA all had introduced cut sites for *AviII*; *pCRII-dmpFG-H203A* vector was the starting point for preparing the H202AH203A variant and the *AviII* cutsite was removed from the H202AH203A DNA sequence. Mutagenized plasmid DNA was sent to Bio S&T (Montreal, Quebec, Canada) for sequencing of the insert region to insure that no unexpected mutations were present. Mass spectrometry of each purified variant protein provided additional verification that the correct variants had been obtained.

Variant	Primer Sequence	Subcloning Fragment
H200A	5'-GCAGGTCGGTATGGCTGCGCACCACAACC-3' 3'-CGTCCAGCCATACCGACGCGTGGTGTTGG-5'	*NotI/SphI*, 350 bp
H202A	5'-GGTATGCACGCTGCGCACAACCTCACGG-3' 3'-CCATACGTGCGACGCGTGTTGGAGTGCC-5'	*NotI/SphI*, 350 bp
H203A	5'-CGGTATGCATGCGCACGCCAACCTCAGCCTTGGC-3' 3'-GCCATACGTACGCGTGCGGTTGGAGTCGGAACCG-5'	*NotI/PauI*, 350 bp
H202AH203A	5'-CGGTATGCATGCGGCGGCCAACCTCAGCC-3' 3'-GCCTACGTACGCCGCCGGTTGGAGTCGG-5'	*NotI/PauI*, 350 bp

Table 1: Construction of DmpFG variants. Mismatches in primer sequence are underlined.

Bacterial growth and protein expression. *E. coli* C41(DE3) (39) was made competent (40) and then 50 µl of cells transformed with 10 ng of DNA of the appropriate pT7.5 based expression plasmid by incubating on ice for 30 minutes. The cells were then plated on LB-agar containing 100 µg/ml carbenecillin and grown overnight at 37°C. The transformants were scraped from the plates, resuspended in a few mL of LB, and inoculated into 6 L of LB containing 100 µg/ml ampicillin. These liquid cultures were grown at 37°C with shaking until the OD_{600} was 0.8-1.0, and then IPTG (Bioshop) was added to a final concentration of 1 mM to induce protein expression. The induced cultures were grown for an additional three hours at 37°C, then harvested by centrifugation and washed once with 50 mM Na^+-K^+ phosphate buffer, pH 7.4, containing 1 mM dithiothreitol (PD buffer). The cell pellet was stored at -80°C prior to the purification procedure.

Protein purification. All purification steps were carried out at 4°C, with modifications from the originally published procedure (11, 13). PD buffer was used throughout the purification.

Preparation of crude extract. Transformed *E.coli* C41(DE3) cells (wet weight, 25-30 g) were suspended in PD buffer (2 ml / g cells) with a spatula-tip of DNase I (grade II, Roche). The cell suspensions were placed in a salt-water bath containing ice, and sonicated in 30-40 ml batches using a Branson Sonifier at 40-60% full power, output of 3-4, for 10 bursts of 15 s each. The resulting lysate was centrifuged for 1 hr at 62,000 x *g* to remove cellular debris, and the supernatant was used as the crude extract.

Fast-Flow DEAE-Sepharose chromatography. After the column was equilibrated with PD buffer, the crude extract was applied at a rate of 6 ml/min. Once the sample was loaded, the column was washed with 100 ml PD buffer then 200 ml of the same buffer containing 50 mM NaCl. To elute DmpG, a linear gradient of 50 mM to 275 mM NaCl in buffer (1,500 ml) was applied and eluted fractions containing peak DmpF dehydrogenase activity were pooled.

Ammonium sulfate fractionation. The pooled fractions from the DEAE-Sepharose column were brought to 55% saturation (33.1 g / 100 ml) with ammonium sulfate and then centrifuged at 23,975 x *g* for 20 min. The protein precipitate was dissolved in a total volume of 5 ml PD buffer, and this preparation was then desalted using two PD-10-desalting columns (Amersham Bioscience) using the manufacturer's suggested protocol.

NAD^+-affinity chromatography. The desalted protein was diluted to 25 ml with PD buffer and loaded on a column of N^6-linked immobilized NAD^+ affinity resin. The solid-phase resin was synthesized by Dr. J. Powlowski using EAH-Sepharose 4B (Amersham) and N^6-

carboxy-methyl-NAD^+ prepared as described by Tynan *et al.* (41). The coupling procedure was as described by Amersham Biosciences. After loading the protein on the column, the column was washed with 30 ml PD buffer and the enzyme was eluted with either 1 mM NAD^+ (Grade I, Roche) or 100 mM NaCl in PD buffer. Eluted fractions with peak DmpF dehydrogenase activity were pooled and then buffer was exchanged by bringing the volume to 50 ml with 50 mM HEPES, pH 8.0, containing 0.5 mM TCEP (Pierce), and concentrating to 5 ml using a stirred Amicon concentrator unit (Millipore) fitted with a YM-30 filter. The buffer exchange procedure was repeated three times and ~ 3 ml of concentrated enzyme solution was aliquoted and stored at -80°C until further use.

Protein methods. The purity of the protein preparations was estimated by SDS-PAGE (21). Subunit molecular masses were confirmed by direct-injection on a Q-TOF 2 (Micromass). To estimate the protein concentration, the BCA assay (Pierce) was used in conjunction with TCA precipitation to remove interfering substances (42). BSA protein supplied with the assay kit was used as the standard to construct a calibration curve. Protein concentration was also estimated from the absorbance at 280 nm using the method of Mach (43).

Electospray ionization mass spectrometry. Subunit molecular masses were confirmed by direct-injection on a Q-TOF 2 (Micromass). Stock enzyme was buffer exchanged into 18.2 MΩ Milli-Q water (Millipore) using a Microcon YM-10 (Millipore) centrifugal device, and brought to a final protein concentration of 1 μM in 50% acetonitrile with 0.2% formic acid before injection. These diluted samples were directly introduced into the spray source at a flow-rate of 1.0 μl/min. The capillary voltage was set at 3800 V; cone voltage 45 V;

multiplier 550 V; MCP 2100 V; TOF -9.1V. Raw spectra were smoothed and deconvolved using the MassLynx software (Micromass).

Inductively coupled plasma mass spectrometry. ICP-MS samples were run by Josiane Lafleur at McGill University, and sample preparation was based on the Tanner method (44). All glassware, microfuge tubes and pipette tips were washed overnight in dilute nitric acid. Purified protein was first desalted on NAP-5 columns (Amersham) that had been rinsed with 1 ml of 0.2 M EDTA then equilibrated with 10 ml of metal-free 50 mM HEPES buffer, pH 8.0, that had been previously treated with Chelex-100 (BioRad). Samples were loaded and then eluted from the NAP-5 column according to manufacturer's protocol, and the final protein concentration was determined using the BCA assay. Eluted DmpFG WT was also assayed for residual aldolase activity in the absence of added metals. The protein was digested for 12 hours at 50°C in 10 % nitric acid, and then diluted in 18.2 MΩ Milli-Q water (Millipore) prior to analysis.

Circular dichroism spectroscopy. Far-UV CD experiments were conducted at room temperature on a Jasco J-710 CD spectrometer purged with N_2 gas (5 L/min). Spectra were acquired in the 200-260 nm region using a scan speed of 100 nm/min and response time of 0.25 s. The far UV/CD spectra reported here are the average of 5 scans at 0.5 nm resolution and a bandwidth of 1.0 nm, all with detector voltages below 700 V. The samples containing urea were incubated for 16 hours at room temperature and all samples were centrifuged briefly to remove any particulate matter. WT and variant native state

comparisons were performed with 0.5 mg/ml protein in 50 mM HEPES, pH 8.0. Urea denatured samples had a protein concentration of 0.2 mg/ml.

Fluorescence spectroscopy. Fluorescence measurements were carried out on an Aminco Bowman series 2 Fluorimeter. Emission spectra were collected between 300 and 400 nm, following excitation at both 280 nm and 295 nm for each sample, and with a bandwidth of 4 nm for both excitation and emission. Samples were centrifuged briefly before placing in a 400 μL cuvette. Data were then collected at a scan speed of 1 nm/sec. WT and variant sample concentration was 0.15 mg/ml, in 50 mM HEPES, pH 8.0. Urea denatured WT samples were in a buffer of 50 mM Na^+-K^+ phosphate, pH 7.4.

Sedimentation velocity analytical ultracentrifugation under native conditions. WT and mutant proteins samples were brought to a concentration of 0.5 mg/ml, 50 mM HEPES, pH 8.0, containing 0.1 M NaCl. Buffer blanks and samples were centrifuged at a speed of 42,000 r.p.m. at a temperature of 20°C using an An-60 Ti rotor Beckman Optima XL-I analytical ultracentrifuge, and scans measuring the absorbance at 280 nm followed the sedimentation process. Distribution plots were constructed using Sedfit v8.5 software (by P. Shuck; http://www.analyticalultracentrifugation.com), fitting raw data to the c(s) and c(M) models. SEDNTERP v1.08 software (http://www.rasmb.bbri.org/; developed by Hayes, Laue and Philo) was used to calculate the buffer v-bar, density, and viscosity to be 0.7389 ml/g, 1.00972 g/ml, and 1.0301 X 10^{-2} (cp), respectively. These values were calculated arbitrarily using 50 mM Na^+-K^+ phosphate, since physical data was not readily available for HEPES.

Sedimentation velocity analytical ultracentrifugation under denaturing conditions. DmpFG WT samples at a concentration of 0.5 mg/ml were incubated overnight in 0, 1.0, 2.5, 3.0, or 4.5 M urea, including 50 mM Na^+-K^+ phosphate buffer, pH 7.4, and 0.1 M NaCl. As with non-denatured samples, buffer blanks and samples were centrifuged at a speed of 42,000 r.p.m. and temperature of 20°C using an An-60 Ti rotor Beckman Optima XL-I analytical ultracentrifuge, and scans measuring the absorbance at A_{280} followed the sedimentation process. Data were analyzed using Sedfit v8.5 software. V-bar, density, and viscosity were calculated using Sednterp v1.08 software as follows: no urea: 0.7389 ml/g, 1.00972 g/ml, 1.0301 X 10^{-2} (cp); 1 M urea: 0.7389 ml/g, 1.02509 g/ml, 1.0685 X 10^{-2} (cp); 2.5 M urea: 0.7389 ml/g, 1.05861 g/ml, 1.1593 X 10^{-2} (cp); 3 M urea: 0.7389 ml/g, 1.06593 g/ml, 1.1733 X 10^{-2} (cp) 4.5 M urea: 0.7389 ml/g, 1.08923 g/ml, 1.2937 X 10^{-2} (cp).

Discontinuous transverse-gradient urea polyacrylamide gels. Gels were prepared essentially as described by Gentile (45). Two gels were poured with 0.5 M urea increments for each lane, 0-4.5 M in one gel and 3.5-8.0 M in the other gel. A counter-gradient of acylamide, 7-4 %, was established over the 0-8 M gradient of urea, to insure homogeneous gel density. After polymerization, samples of DmpFG protein were brought to 0.1 mg/ml with 2X native sample buffer (0.5 M Tris buffer, pH 8.9, with 20 % glycerol and 0.02 % bromomphenol blue) and then applied to gel wells. The gel was run for 12 hours at a constant current of 4 mA. For the gel at pH 7.4, a HEPES/imidazole buffer was used (46). Gels were stained and destained by standard procedure (47).

Identification of gel bands in tranverse-gradient urea polyacrylamide gels. Fragments of the urea gel were excised with a scalpel and mixed with 50 µl of 2X sample buffer (125 mM sodium phosphate buffer, pH 7.4, with 200 mM DTT, 20 % glycerol, 4 % SDS, and 0.02 % bromophenol blue). The samples were homogenized with a thin glass stir rod and then centrifuged briefly. The liquid supernatant was boiled for 3-5 minutes and applied to SDS-PAGE (12 % acrylamide) (47) and the resulting SDS-gels were stained using a silver-staining kit (Pharmacia). The presence of either or both DmpF and (32.5 kDa) and DmpG (37.5 kDa) subunits was confirmed by visual examination.

Analysis of DmpFG precipitate formed during incubation with guanidine·HCl. DmpFG was diluted to 0.5 mg/ml in 50 mM HEPES, pH 8.0, and samples containing no Gd·HCl, 0.4 M, 0.8 M, 1.2 M, or 2.0 M Gd·HCl and 0.8 M Gd·HCl with 1 M urea, were prepared. The samples were incubated for 30 min at room temperature, and then centrifuged at maximum speed for 15 min in a microfuge. The supernatant was removed, and 100 µl of 1X running buffer (25 mM Tris, 19.2 mM glycine, 0.1 % SDS) was used to resolubilize any pellet that was formed, by pipetting up and down a number of times. A 10 µl aliquot of this solution for each sample was removed and mixed with 10 µl of 2X sample buffer (125 mM sodium phosphate buffer, pH 7.4, with 200 mM DTT, 20 % glycerol, 4 % SDS, and 0.02 % bromophenol blue), boiled for 3-5 minutes, then applied to SDS-PAGE for analysis.

Analysis of DmpFG solubility at various temperatures. DmpFG was diluted to 1 mg/ml in 50 mM HEPES, pH 8.0, and incubated at room temperature, 54°C, and 80°C, for one

hour. The samples were then centrifuged for 15 min at room temperature. The supernatants were removed, 10 µl of water and 10 µl of 2X sample buffer (125 mM sodium phosphate buffer, pH 7.4, with 200 mM DTT, 20 % glycerol, 4 % SDS, and 0.02 % bromophenol blue) were added to resolubulize any pellet that was formed, by pipetting up and down a number of times. To the supernatants, 10 µl of the 2X sample buffer was added. All samples were boiled for 3-5 minutes, then applied to SDS-PAGE for analysis.

Enzyme activity assays. All assays were carried out using a Cary Bio50 spectrophotometer thermostated at 25°C, with 50 mM HEPES, pH 8.0 as the assay buffer, unless indicated otherwise.

Coupled DmpF acetaldehyde dehydrogenase (acylating) assays. For assaying fractions associated with the purification procedure, assay mixtures used 50 mM Na^+-K^+ phosphate buffer, pH 7.4 as the buffer, containing 300 µM NAD^+, 100 µM CoA, and 20 mM acetaldehyde, and were performed at room temperature. These assays measured the CoA-stimulated reduction of NAD^+ (A_{340}) (12). In the case of WT and mutant comparisons, 60 nM of enzyme was used, along with 50 mM HEPES buffer, pH 8.0, (in place of Na^+-K^+ phosphate buffer) and the assays were performed at 25°C.

Coupled DmpG–LDH activity assays. In 50 mM HEPES, pH 8.0, 240 µM NADH was mixed with excess LDH (27.5 U), 60 µM of *L(S)*-4-hydroxy-2-ketovalerate, and either 1 mM $MnCl_2$ (or $CoCl_2$), and the reaction was initiated by the addition of 60 nM DmpFG enzyme . The reaction followed the oxidation of NADH (A_{340}) by LDH, which reduces the pyruvate formed by the aldolase reaction of DmpG (12).

***DmpFG coupled assays*:** In 50 mM HEPES, pH 8.0, 600 μM NAD^+, 200 μM of CoA, 60 μM of *L(S)*-4-hydroxy-2-ketovalerate, and 1 mM $MnCl_2$ (or $CoCl_2$) were mixed, and the reaction was initiated by the addition of 60 nM DmpFG enzyme. As with the DmpF assays, CoA-stimulated reduction of NAD^+ was measured (A_{340}), but acetaldehyde was provided to DmpF by means of the DmpG aldolase activity.

Preparation and quantitation of the aldolase substrate, 4-hydroxy-2-ketovalerate. Mild hydrolysis of 4-methyl-2-oxobutyrolactone (48) gave a racemic mixture of *L(S)*- and *R(D)*-4-hydroxy-2-ketovalerate, the *L(S)*- isomer being the substrate for DmpG (12). The concentration of *L(S)*-4-hydroxy-2-ketovalerate was determined using the DmpFG coupled assay. The reaction was followed spectophotometrically for 50 minutes (essentially to completion), and the total amount of NADH measured correlated to the starting concentration of the substrate.

Estimation of kinetic constants. Enzymatic rates measured for DmpG aldolase activity (DmpG-LDH and DmpFG coupled assays) were converted from A_{340}/min to μM/min using an extinction coefficient of 6220 $cm^{-1}M^{-1}$, then fit to the Michaelis–Menten equation with Grafit v4.0 software (Erithacus). With the software, Lineweaver-Burk plots were constructed from non-linear regression fitting of the rate data, and kinetic constants such as apparent V_{max} and K_M for 4-hydroxy-2-ketovalerate were obtained from the fitted parameters.

Oxalate inhibition of coupled DmpFG activity. Various concentrations of oxalate were added to DmpFG coupled assays. In 50 mM HEPES, pH 8.0, 600 μM NADH, 200 μM CoA, 60 μM of *L(S)*-4-hydroxy-2-ketovalerate, 1 mM $MnCl_2$ (or $CoCl_2$), and varying oxalate concentrations were mixed, and the reaction was initiated by the addition of 60 nM DmpFG enzyme. CoA-stimulated reduction of NAD^+ was measured (A_{340}). Activity level in the absence of oxalate was considered to be 100%, and plotting assay data using the IC50 model in Grafit v4.0 software (Erithacus) gave an estimation of the concentration of oxalate which gives 50% activity.

RESULTS

Purification of DmpFG WT and variants

All enzymes, namely DmpFG WT, and aldolase variants H200A, H202A, H203A, and H202AH203A were expressed and purified by identical methods as described in "Materials and Methods"). Briefly, plasmid DNA containing the genes for DmpFG WT and variants were engineered and silent restriction sites introduced by mutations in the DNA were confirmed by restriction digest. *E. coli* cells were transformed with the plasmids containing the corresponding genes, protein expression induced by IPTG, and cells harvested. The resulting cell paste (~25-30 g) was resuspended, disrupted, and subjected to ultracentrifugation. DEAE column chromatography, ammonium sulfate precipitation and NAD^+-affinity column chromatography were subsequently applied to the crude extract to purify DmpFG.

Table 1 summarizes the purification results for WT and variants in terms of protein content and dehydrogenase activity yields; Figure 7 demonstrates the protein purity observed after each purification step: although data is shown only for WT, these results represent typical purities for variant preparations as well. The H200A variant was a slight exception, since a small amount of low molecular mass (~20 kDa) impurity was identified by SDS-PAGE following the NAD^+-affinity chromatography step (data not shown); the impurity was subsequently removed by reapplication of the enzyme to a DEAE column as was described for the first part of the purification procedure . ESI-MS revealed expected subunit masses

for DmpF and DmpG (WT and variants) ± 2 Da. The average experimental mass of DmpF was

	WT	Variants			
		H200A	**H202A**	**H203A**	**H202AH203A**
Supernatant (total Units)	2840	1740	2360	1590	2430
DEAE pool (total Units)	1620	1740	3010	1960	3390
Affinity pool (total Units)	510	700	1800	630	670
Activity yield (%)	18	40	76	40	28
Protein yield (mg)	16.9	16.1	21.7	17.3	23.6

Table 2: Purification summary for DmpFG WT and variants H200A, H202A, H203A and H202AH203A. Activity units refer to assayed dehydrogenase (DmpF) activity, where 1 U = 1 uM/min NAD^+ converted to NADH, and total units is based on the volume of pooled enzyme. DEAE fractions collected were assayed for dehydrogenase activity, and pooled on the basis of high activity vs. low A_{280}. Affinity chromatography fractions were pooled on the basis of dehydrogenase activity only, since the NAD^+ used to elute the sample interferes with protein absorbance at 280 nm. Activity assays were conducted in 50 mM sodium phosphate buffer, pH 7.4.

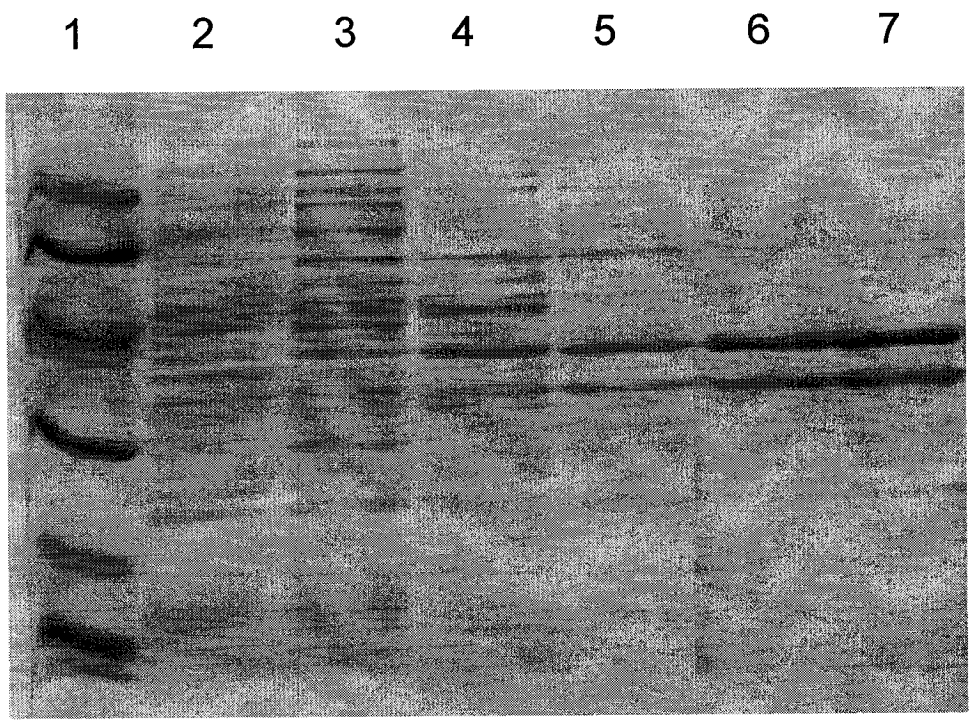

Figure 7: SDS-PAGE gel (12%) demonstrating the purity of a recombinant DmpFG WT preparation after different purification steps. Lane 1: Low molecular weight standards, 94 kDa, 67 kDa, 43 kDa, 30 kDa, 20.1 kDa and 14.4 kDa. Lane 2: crude extract (1:40). Lane 3: supernatant collected after ultracentrifugation (1:20). Lane 4: DEAE column pool . Lane 5: Affinity column pre-load (1:5). Lane 6: Affinity pool Lane 7: Purified DmpFG, concentrated stock (1:20); upper and lower bands correspond to DmpG (37.5 kDa) and DmpF (32.5 kDa), respectively.

32,684 Da; the mass of DmpG WT was 37,340 Da, H200A, H202A and H203A variants were 37,274 Da and the H202AH203A variant was 37,207 Da. The N-terminal methionine was missing from the WT DmpG subunit as previously suggested (11), and was also found to be processed in the four variants.

Biophysical comparisons of DmpFG WT and variants

All purified DmpFG enzymes were subject to circular dichroism spectroscopy, sedimentation velocity analytical centrifugation, and fluorescence spectroscopy in order to compare the WT and variant structural characteristics. The aim was to verify that the variants were correctly folded proteins that existed in tetrameric form, similar to WT.

Far-UV CD indicated that the WT and variants were all correctly folded and had similar secondary structures. The spectra recorded in the 260-210 nm region were all virtually indistinguishable (Figure 8).

Sedimentation velocity analytical ultracentrifugation experiments demonstrated that DmpFG WT and all variants sedimented mainly as single species with a sedimentation coefficient ~ 6.0 S (Figure 9A), corresponding to the tetrameric DmpFG of 140 kDa mass (Fig. 9B) It is unclear whether or not the small differences in S for the major sedimenting species is attributable to conformational differences between the WT and variants. For some variants, especially H203A and H202AH203A, relatively small proportions of species with sedimentation coefficients of ~ 3.0 S were detected. These results suggest that mutations may have slightly destabilized the tetrameric form, so that some dimeric or monomeric form was detected.

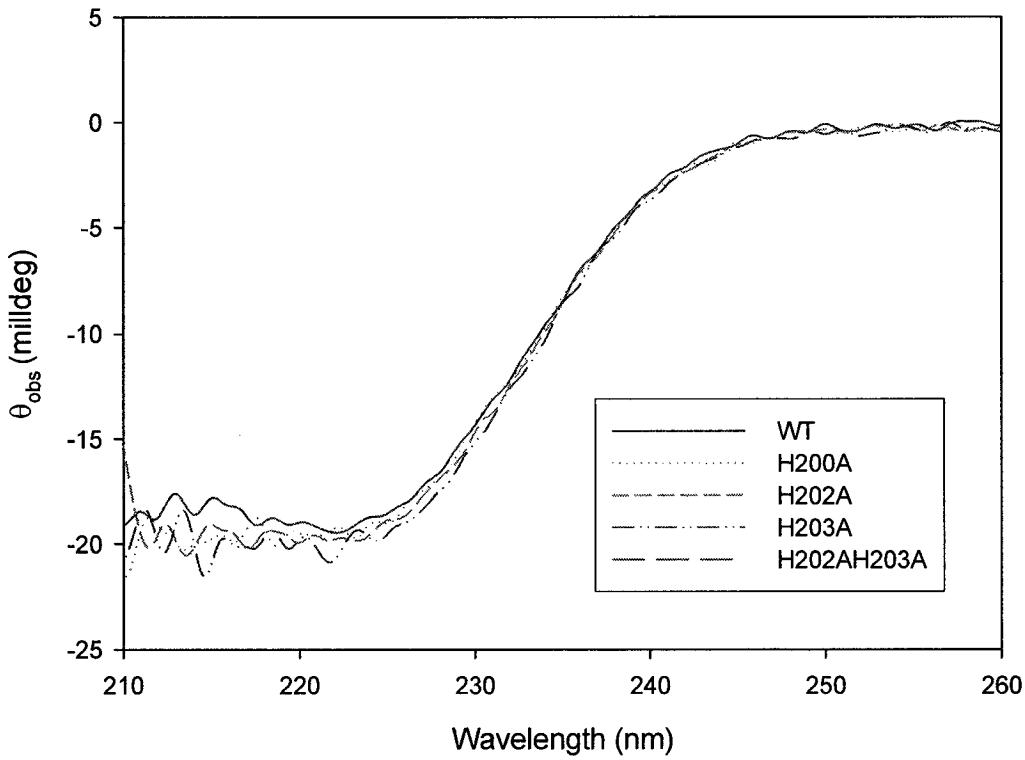

Figure 8: Far-UV CD spectra of DmpFG WT and variants. Protein concentration was 0.4 mg/ml in 50 mM HEPES, pH 8.0; samples were scanned in a cell of pathlength 0.5 mm.

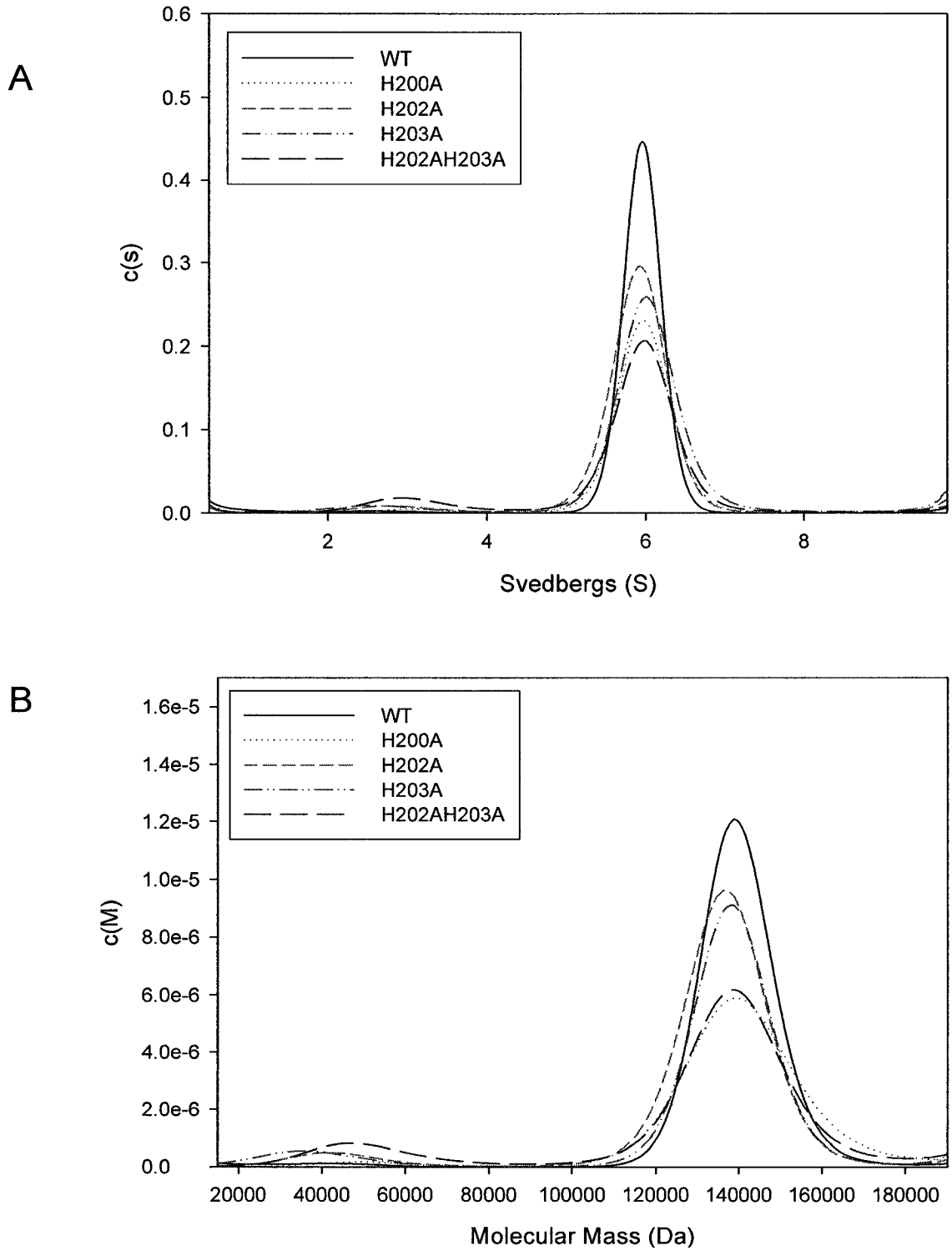

Figure 9: Sedimentation velocity AUC data for DmpFG WT and variants. Data were analyzed and plot distribution was constructed using the A) c(s) model and B) C(M) model of Sedfit v8.5 software. Protein concentration was 0.5 mg/ml in 50 mM HEPES, pH 8.0; scans were collected by measuring A_{280} at 42,000 r.p.m., 20 °C.

Fluorescence spectroscopy revealed that DmpFG WT and mutants had different emission profiles when excited at either 280 or 295 nm. At both excitation wavelengths, emission spectra of WT and H203A are the most similar, and the emission intensities of the other variants were significantly increased over WT (Figure 10). Excitation at 295 nm gave a $\lambda_{max} \sim 328$ nm for all of the enzymes. When excited at 280 nm however, the emission of H200A is red-shifted by 10 nm to 322 nm from the approximate emission λ_{max} of 312 nm, which is representative of WT and the other proteins.

The techniques used for biophysical analyses reveal that although the relative secondary and quaternary structures (from CD and AUC results, respectively) are quite similar among the DmpFG enzymes studied, the tertiary structure (from fluorescence results) is the most varied in comparison of the WT to the variants.

Kinetic analysis of the DmpFG WT and variants

DmpF (Dehydrogenase) Activity

The DmpF subunit was relatively unaffected by any of the mutations in the DmpG subunit, as high specific activity for the dehydrogenase could be detected in preparations of all enzymes studied in this report (Figure 11). This observation proved useful in the purification of all the enzymes studied, since the presence of dehydrogenase activity was a criterion for pooling column fractions (see Table 2). H200A, H202A and H202AH203A variants specific activities for the dehydrogenase were notably higher than the WT or

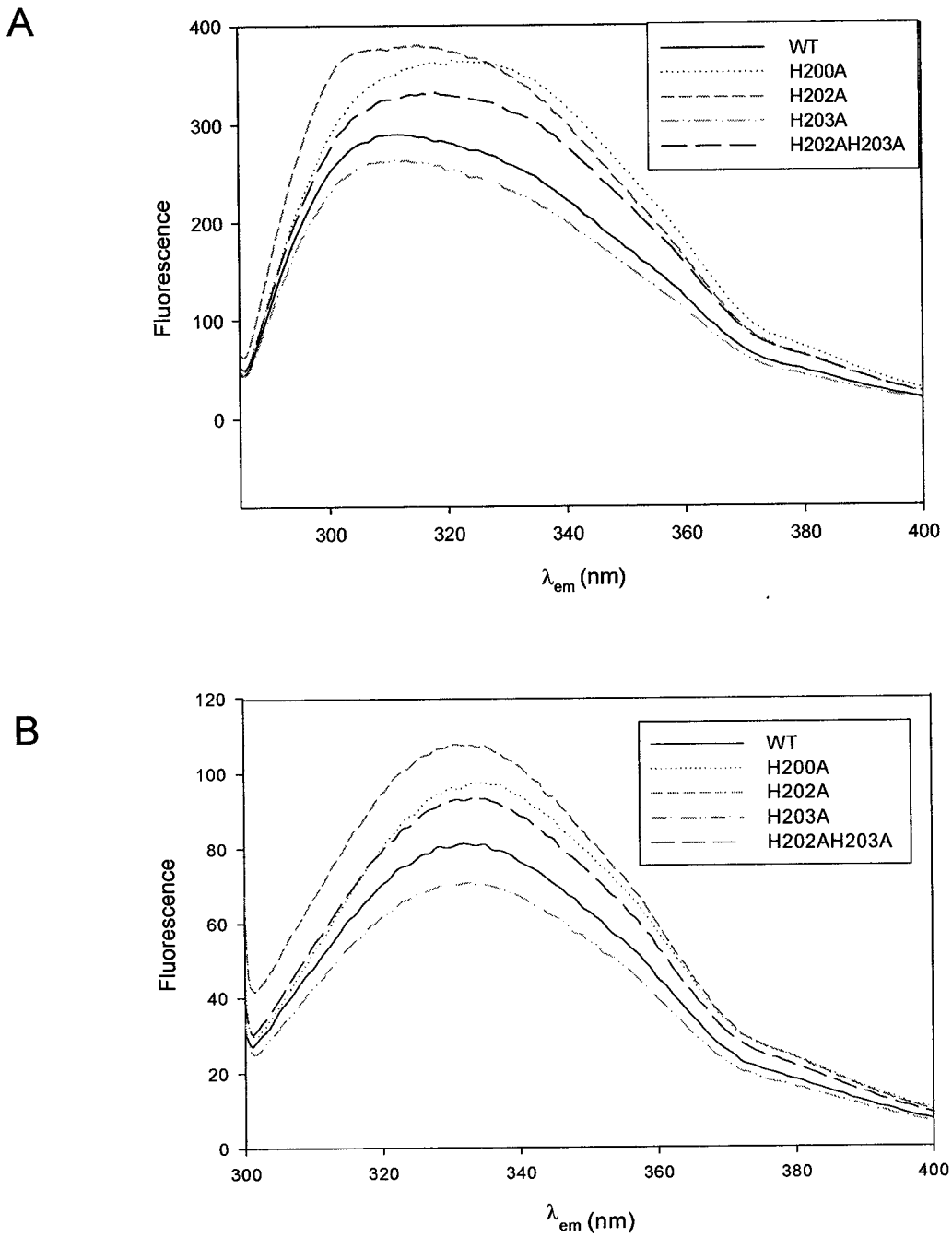

Figure 10: Fluorescence emission spectra of DmpFG WT and variants. Emission spectra of proteins excited by light of A) 280 nm wavelength and B) 295 nm wavelength. Protein concentration was 0.15 mg/ml in 50 mM HEPES, pH 8.0, measured using a 400 µl quartz fluorescence cuvette.

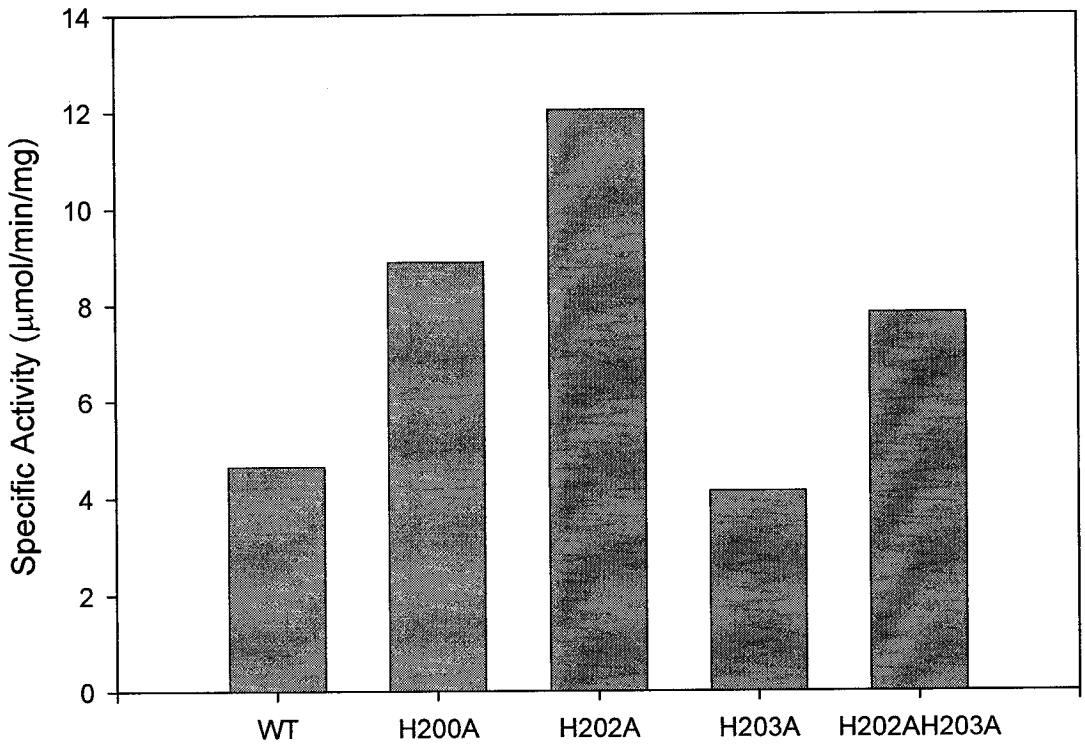

Figure 11: Dehydrogenase (DmpF) activity measurements of WT and variants. Assays were conducted in 50 mM HEPES, pH 8.0. See *Materials and Methods* section for details. Assays were performed in duplicate, and the average was graphed.

H203A enzymes, with the H202A variant exhibiting greater than two-fold increase over WT (Figure 11).

DmpG (Aldolase) Activity

As previously reported (11), the WT DmpFG exhibited some residual aldolase activity that was stimulated somewhat upon addition of Mn^{2+}, but in all mutants except for H203A, this basal level of activity was absent (Figure 12). In the presence of 1 mM $MnCl_2$, aldolase activity was increased for WT, and detectable in all variants except for H200A. Although the results in Figure 12 are based on DmpFG coupled assays, Mn^{2+}-stimulated H200A aldolase activity was also absent when using the LDH-coupled DmpG assay. Neither a 3-fold higher enzyme concentration (20 μg/ml) nor increased Mn^{2+} concentration (10 mM) could elicit any detectable aldolase activity in the H200A mutant.

Some recent publications have suggested that a class II fructose-1,6-bisphosphate aldolase from *Thermus aquaticus* uses Co^{2+} for activity (17). Other metals that had been previously tested with WT (1 mM) were Ca^{2+} and Mg^{2+} which had no effect, and Zn^{2+} which was strongly inhibitory (11). However, no previous attempts were made to stimulate aldolase activity of the DmpFG complex with Co^{2+} (J. Powlowski, personal communication). Addition of 1 mM $CoCl_2$ to coupled DmpFG assays demonstrated that Co^{2+} could stimulate activity at levels equal to, or higher than, observed with Mn^{2+} (Figure 12). Interestingly, Co^{2+} stimulated aldolase activity in the H200A variant, whereas Mn^{2+} did not.

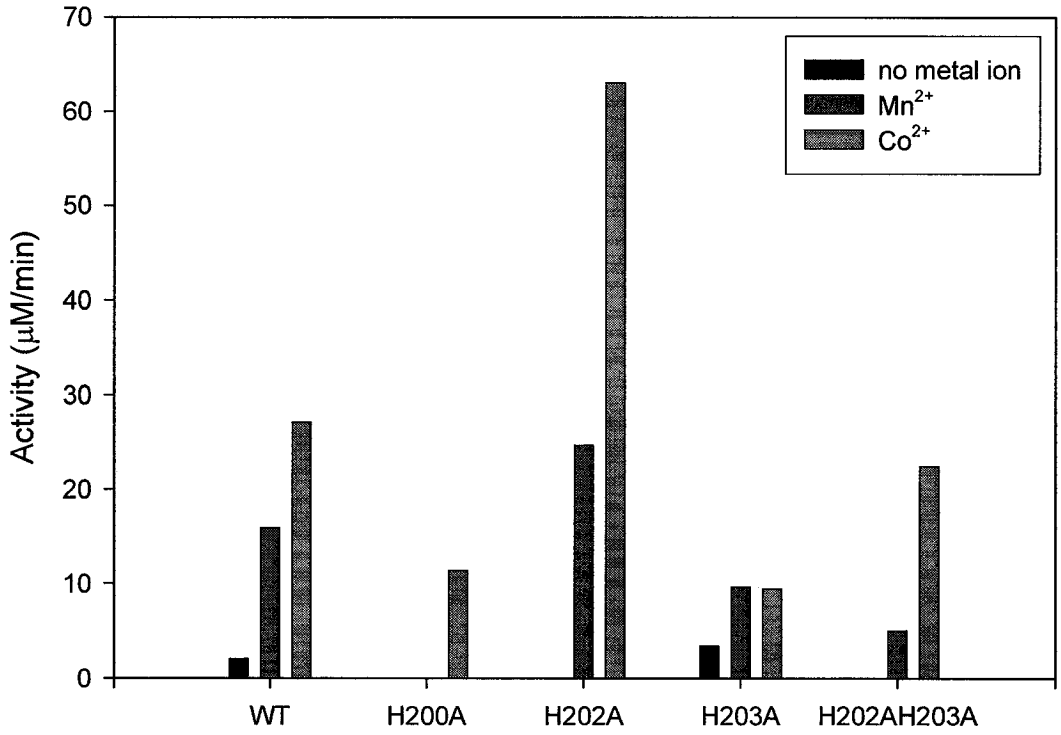

Figure 12: DmpFG coupled assays for DmpFG WT and variants +/- 1mM $MnCl_2$ or $CoCl_2$. See *Materials and Methods* for assay details. Enzyme content of the assay was 8.3 μg. All assay components were kept constant, with the exception of added metal ion. Assays were performed in duplicate, and an average is reported.

DmpG (aldolase) steady state kinetics

Certain mutations of proposed active site residues in HMG-CoA lyase resulted in drastic changes in k_{cat} and K_M for substrate (32, 33), so determining if the DmpFG variants had altered kinetic parameters as compared to WT was of interest. Using the DmpFG coupled assays, DmpFG H200A, H202A were determined to have elevated values over WT of both apparent k_{cat} and $K_{M,\ app.}$ for 4-hydroxy-2-ketovalerate over WT (Figure 13, Table 3). The $K_{M,\ app.}$ differences were the most notable, increasing almost 2 orders of magnitude for H202AH203A. The $K_{M,\ app.}$ of the H203A variant was, however, not markedly different than WT, although the k_{cat} was decreased several-fold. The kinetics of the H202AH203A variant were most like those of H200A and H202A, having both increased k_{cat} and $K_{M,\ app}$ values. There is currently no clear explanation for the increased k_{cat} in H200A, H202A and H202AH203A variants, but the issue will be further addressed in the "Discussion".

The kinetic parameters obtained using the coupled DmpFG assays (Figure 13, Table 3) and coupled DmpG-LDH assays (Figure 14, Table 4) were reasonably similar, with the main exception being the difference in $K_{M,\ app}$ calculated for the H202A variant. The $K_{M,\ app.}$ determined by the coupled DmpG-LDH assay was increased as much as 10-fold.

A

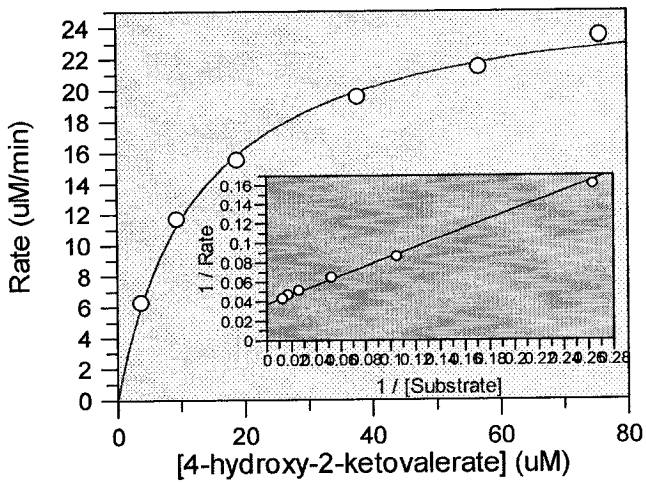
Rate (uM/min)
[4-hydroxy-2-ketovalerate] (uM)
1 / Rate
1 / [Substrate]

B

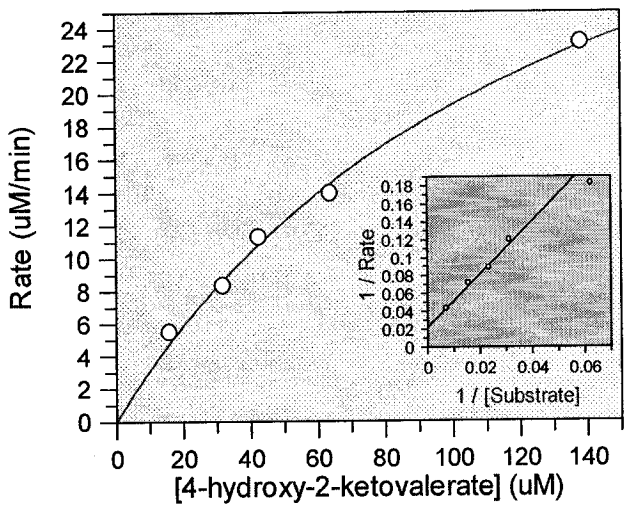
Rate (uM/min)
[4-hydroxy-2-ketovalerate] (uM)
1 / Rate
1 / [Substrate]

C

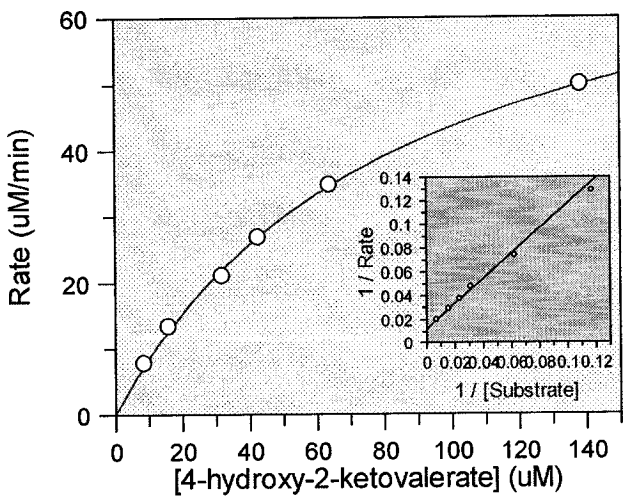
Rate (uM/min)
[4-hydroxy-2-ketovalerate] (uM)
1 / Rate
1 / [Substrate]

D

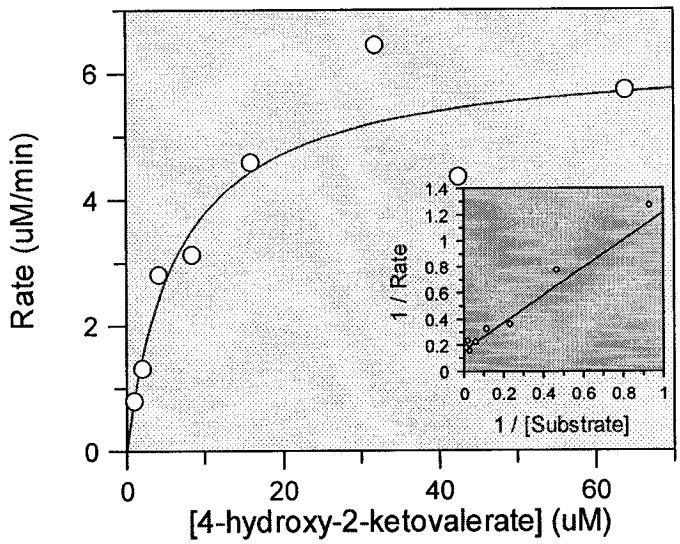

E

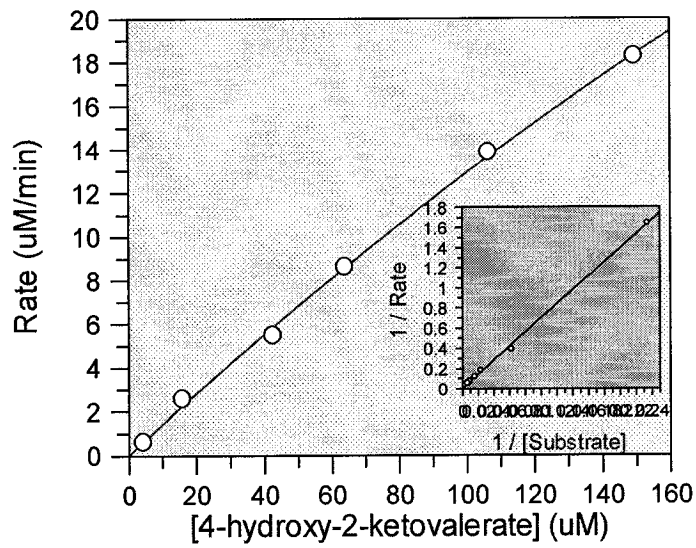

Figure 13: Steady state kinetics of DmpFG WT and variants using the DmpFG coupled assay. Kinetic profiles are illustrated for DmpFG A) WT B) H200A, C) H202A D) H203A and E) H202AH203A. Double reciprocal plots for determination of apparent k_{cat} and K_M for 4H2KV (Table 3) are inset. Concentrations of assay components were constant, with the exception of varied 4H2KV substrate concentration. Activity assays for H200A were done in the presence of 1 mM $CoCl_2$; all others were done using 1mM $MnCl_2$.

	$k_{cat, app.}$ (s^{-1})	$K_{M, app.}$ (μM)	k_{cat}/K_M ($M^{-1}s^{-1}$)
WT	7.41 ± 0.17	12.94 ± 1.02	5.73 X 10^5
H200A*	12.61 ± 1.22	135.39 ± 21.33	9.31 X 10^4
H202A	22.34 ± 0.73	84.79 ± 5.17	2.63 X 10^5
H203A	1.75 ± 0.18	6.64 ± 2.42	2.64 X 10^5
H202AH203A	34.06 ± 9.15	850.52 ± 260.22	4.00 X 10^4

Table 3: Summary of the apparent steady-state kinetic parameters for DmpFG WT and variants, based on the DmpFG coupled assay. The K_M and k_{cat} are apparent, since assays were not necessarily done in the presence of saturating concentrations of metal ion.

*Assays carried out in the presence of Co^{2+} since no activity was observed in the presence of Mn^{2+}.

A

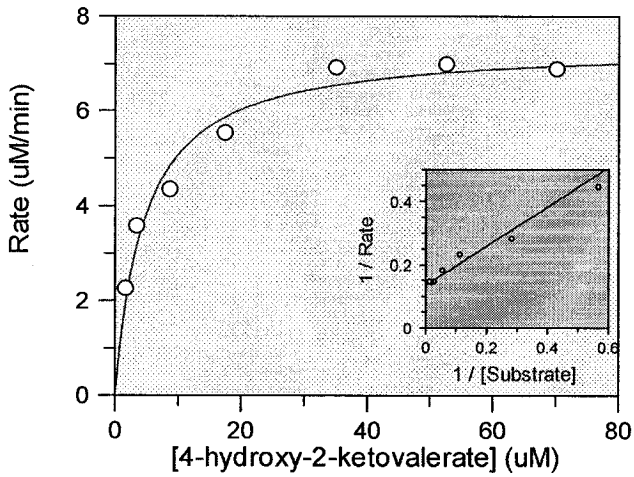
Rate (uM/min)
[4-hydroxy-2-ketovalerate] (uM)
1 / Rate
1 / [Substrate]

B

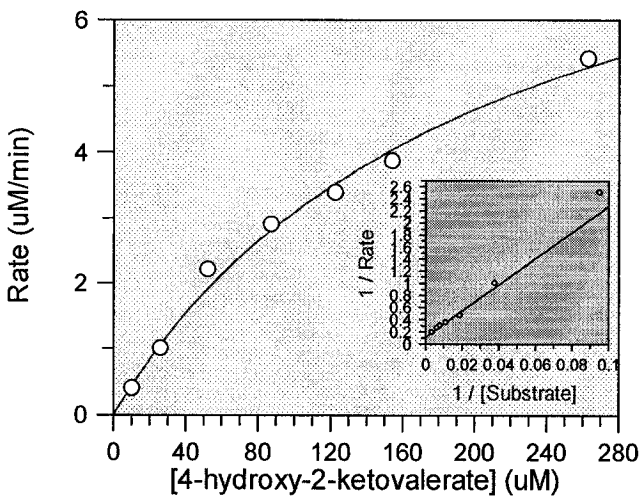
Rate (uM/min)
[4-hydroxy-2-ketovalerate] (uM)
1 / Rate
1 / [Substrate]

C

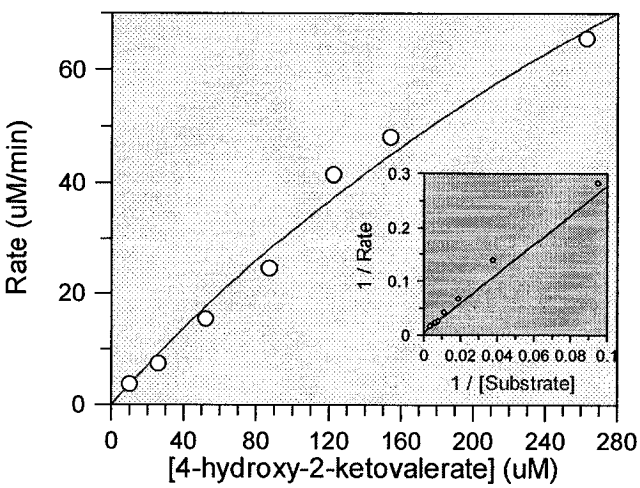
Rate (uM/min)
[4-hydroxy-2-ketovalerate] (uM)
1 / Rate
1 / [Substrate]

D

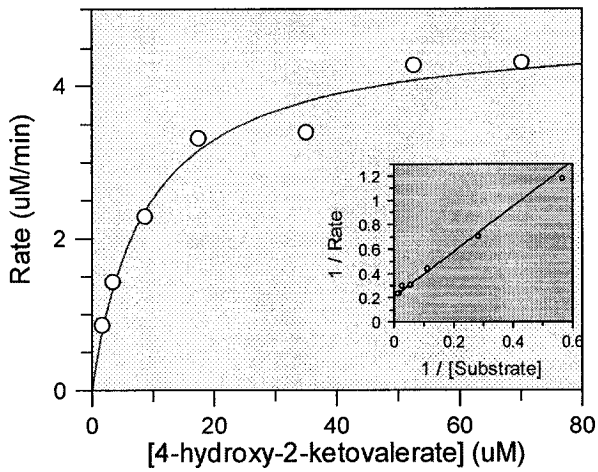

E

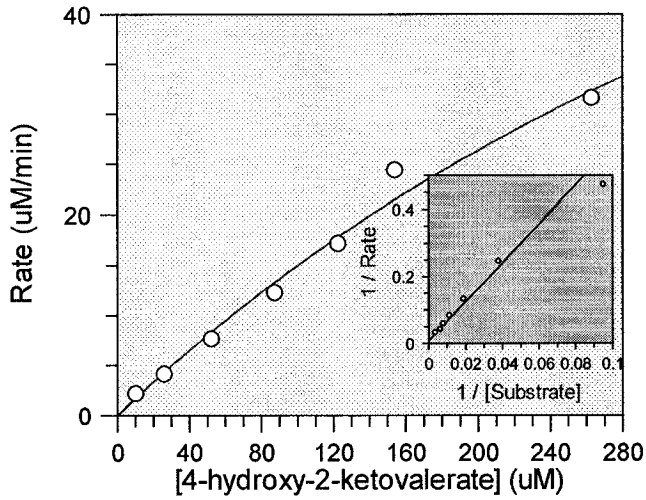

Figure 14: Steady state kinetics of DmpFG WT and variants using the DmpG-LDH coupled assay. Kinetic profiles are illustrated for DmpFG A) WT B) H200A, C) H202A D) H203A and E) H202AH203A. Double reciprocal plots for determination of apparent k_{cat} and K_M for 4H2KV (Table 4) are inset. Concentrations of all assay components were constant, with the exception of varied 4H2KV substrate concentration. The concentration of enzyme for H203A assays was 3X greater than the others because of low specific activity. Activity assays for H200A were done in the presence of 1 mM $CoCl_2$; all others were done using 1 mM $MnCl_2$.

	$k_{cat, app.}$ (s^{-1})	$K_{M, app.}$ (μM)	k_{cat}/K_M ($M^{-1}s^{-1}$)
WT	2.06 ± 0.08	4.60 ± 0.79	4.35×10^5
H200A*	2.60 ± 0.27	203.88 ± 36.92	1.27×10^4
H202A	61.22 ± 21.42	600.89 ± 275.19	1.02×10^5
H203A	0.47 ± 0.02	8.78 ± 1.55	5.35×10^4
H202AH203A	31.00 ± 11.09	647.39 ± 297.32	4.79×10^4

Table 4: Summary of the kinetic parameters calculated for DmpFG WT and variants, based on the DmpG-LDH assay. The K_M and k_{cat} are apparent, since assays were not necessarily done in the presence of saturating concentrations of metal ion.

*Assays carried out in the presence of Co^{2+} since no activity was observed in the presence of Mn^{2+}.

Metal ion concentration dependence of aldolase activity in DmpFG WT and variants

The enzymes were assayed for aldolase activity with varying concentrations of $MnCl_2$ or $CoCl_2$, since Mn^{2+} and Co^{2+} are the only two known activators of activity (see Figure 12). The DmpG-LDH assay was used exclusively, since preliminary results using the DmpFG coupled assay indicated slight turbidity in the assay solution at higher metal ion concentrations (> 5 mM). Increasing the metal ion concentration for the WT (Figure 15A) and variants (Figure 15B-E), does not result in activity that follows Michaelis-Menten kinetics, as there appears to be multiple events occurring. The general trend in each case is metal ion stimulation of activity, which appears to saturate at around 1 mM, but activity then increases at higher metal ion concentrations. Following the reactions to completion gave expected product yields, ruling out the possibility that assay components are precipitating (i.e.: by forming complexes in the presence of high metal ion concentrations) and causing increased absorbance readings. To eliminate the possibility of ionic strength changes having an effect on aldolase activity, assays were carried out in the presence and absence of salt. A concentration of 5 mM NaCl did not appear to have an effect on activity of WT either in the presence or absence of 1 mM Mn^{2+} (data not shown).

DmpFG WT showed relatively little discrimination between Co^{2+} or Mn^{2+} at lower concentrations, but a marked preference for Mn^{2+} at metal ion concentrations above 0.6 mM; compared to activity in the absence of added metal ions, there was a ~10-fold stimulation by 10 mM Co^{2+} and a 20-fold stimulation by 10 mM Mn^{2+} (Figure 15). The H203A variant was only very slightly stimulated by increasing either Co^{2+} or Mn^{2+}, only about 2-fold upon addition of 10 mM of either metal ion, and still resulting in less than 10

% of WT activity. H202A and H202AH203A variants preferred Co^{2+} at all concentration examined, exhibiting 2-3 fold higher activity than with Mn^{2+}; at metal ion concentrations of 5-10 mM, the activity appeared to be slightly inhibited, a result not observed for the other enzymes (Figure 15C & E). The H200A variant can only be stimulated by Co^{2+}, and was while experiencing only modest stimulation below 0.6 mM Co^{2+}, the activity was doubled between 0.6 and 1.2 mM and quadrupled by 10 mM Co^{2+} (Figure 15B). Only WT and H203A demonstrated measurable activity in the absence of added metal ion.

Oxalate inhibition of coupled DmpFG activity

Because of oxalate's structural similarity to 4-hydroxy-2-ketovalerate or pyruvate and its possible presence at the active site revealed by crystal structure analysis, the potential use of oxalate as an inhibitor of aldolase activity was examined. $IC50_{oxalate}$ concentrations were obtained. Coupled DmpFG assays were used exclusively over coupled DmpG-LDH assays, since LDH is known to be inhibited by oxalate (Roche, product insert for LDH). DmpFG WT and the H203A variant were the most strongly inhibited by oxalate, followed by the H202A, H202AH203A and H200A variants. The H200A variant had an $IC50_{oxalate}$ concentration that was roughly 80X greater than WT (Table 5). While it is most likely that oxalate behaves as a competitive inhibitor with the 4-hydroxy-2-ketovalerate substrate or pyruvate product, current results cannot confirm such a hypothesis, and other types of oxalate-mediated inhibition are also possible. Nevertheless, H200A, H202A and H202AH203A variants have increased $IC50_{oxalate}$ over WT and the H203A variant, which is a trend similar to their increased K_M's for 4-hydroxy-2-ketovalerate.

A

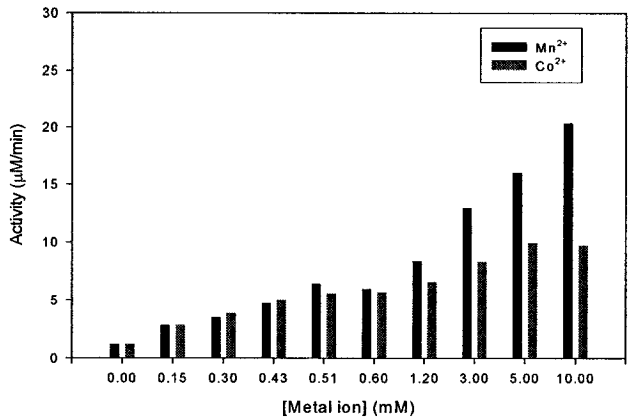
Mn2+
Co2+
Activity (µM/min)
30
25
20
15
10
5
0
0.00 0.15 0.30 0.43 0.51 0.60 1.20 3.00 5.00 10.00
[Metal ion] (mM)

B

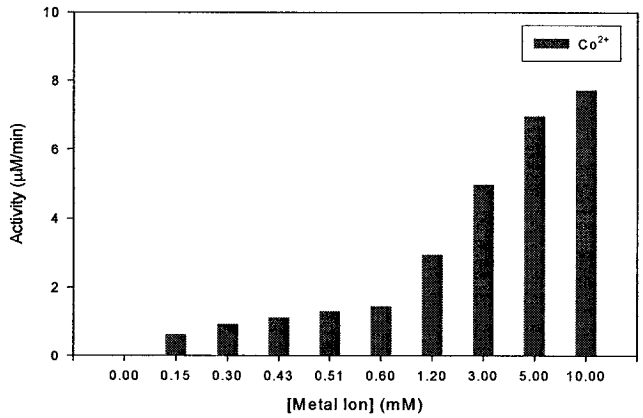
Co2+
Activity (µM/min)
10
8
6
4
2
0
0.00 0.15 0.30 0.43 0.51 0.60 1.20 3.00 5.00 10.00
[Metal ion] (mM)

C

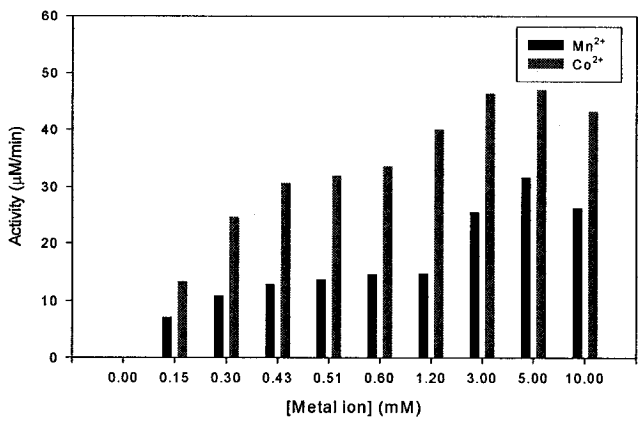
Mn2+
Co2+
Activity (µM/min)
60
50
40
30
20
10
0
0.00 0.15 0.30 0.43 0.51 0.60 1.20 3.00 5.00 10.00
[Metal ion] (mM)

D

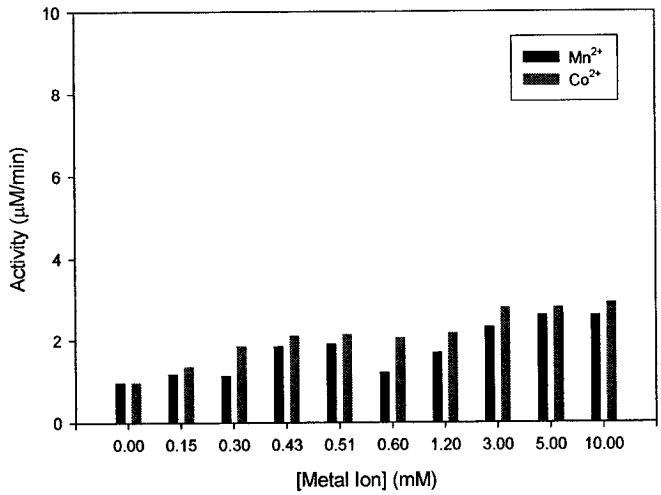

E

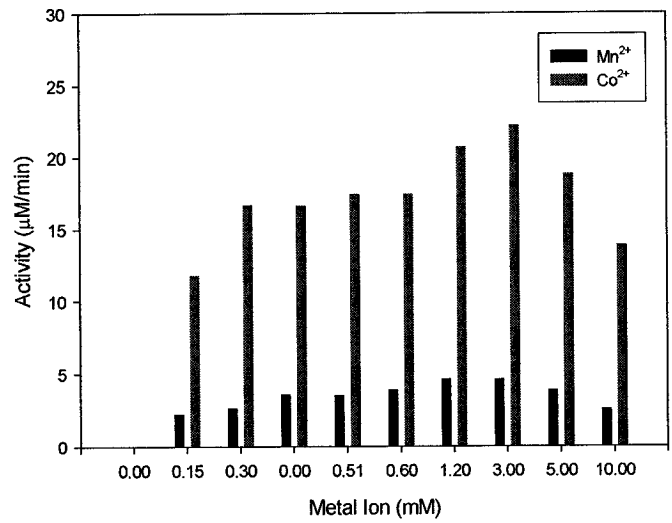

Figure 15: Aldolase activity measurements to demonstrate the metal ion concentration dependence of DmpFG and variants for Mn^{2+} and Co^{2+}. Assays were carried out for DmpFG A) WT, B) H200A, C) H202A, D) H203A and E) H202AH203A. The concentrations of all assay components were held constant, except the metal ion concentration. Note that results for H200A are shown for Co^{2+} only, since aldolase activity of H200A with Mn^{2+} was not detected. Results are shown for single assays, although several duplicates were obtained at various metal ion concentrations to ensure reproducibility.

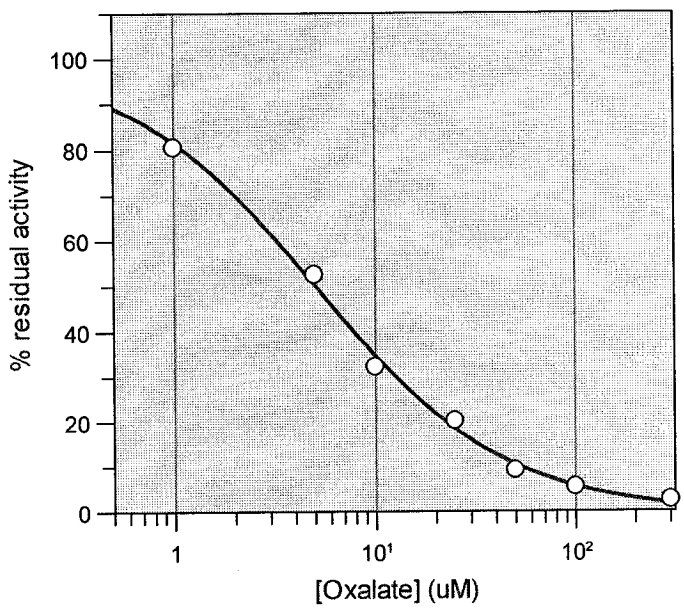

Figure 16: Kinetic analysis for IC50 determination of oxalate inhibition of coupled DmpFG activity. The inhibition profile is illustrated for DmpFG WT only, but represents similar data obtained for the variants. Components of DmpFG coupled assays were invariable, with the exception of varied oxalate concentration. The concentration of enzyme for H202AH203A assays was 3X greater than the others because of low specific activity. Activity assays for H200A were done in the presence of 1 mM $CoCl_2$; all others were done using 1mM $MnCl_2$.

	$IC50_{oxalate}$ (μM)
WT	5.15 ± 0.49
H200A*	404.91 ± 102.03
H202A	26.74 ± 1.74
H203A	10.45 ± 1.55
H202AH203A	123.77 ± 13.49

Table 5: Summary of IC50 determinations for oxalate inhibition of DmpFG WT and variants. These data were based on results obtained using DmpFG coupled assays that contained varying amounts of oxalate.

*Assays carried out in the presence of Co^{2+} since no activity was observed in the presence of Mn^{2+}.

Metal analysis of DmpFG WT and variants

Table 6 shows the results of the analysis of metal content of the various purified enzymes based on ICP-MS. WT and H203A enzymes appear to have the highest metal content with 1.01 and 0.95 eq. respectively, of metal bound per DmpG subunit. These data are consistent with the crystallographic analysis, which indicates 1 metal ion bound per DmpG. Previous ICP-MS experiments done on WT by Dr. L. Sahlman of our laboratory showed Mn as the most abundant metal, but the results shown in Table 6 indicate that little Mn was detected, (0.12 eq.) and more Zn (0.26 eq.) and Fe (0.59 eq) were present instead. Several changes in purification protocol (i.e.: switching to *E.coli* expression strain C41(DE3) from the previous BL21(DE3) strain) may account for these differences (see "Discussion"). His203 is unlikely to be a metal ligand, based on x-ray structure, and metal ion content is similar to WT (Table 6). The content of the H203A variant was mainly Fe (0.47 eq.) and Zn (0.46 eq.) with very little Mn (0.02 eq.). H200A had less metal bound than WT, with 0.66 eq of total metal ion bound, with 0.43 eq. Cu and 0.23 eq. Fe. H202A and H202AH203A samples were almost completely devoid of metal, having totals of 0.08 and 0.18 eq. respectively. Although Co^{2+} was determined to be a potent activator of aldolase activity (Figure 12), no Co was detected in any of the samples.

Sample	Manganese	Cobalt	Magnesium	Copper	Zinc	Cadmium	Nickel	Iron
	mol eq. metal / DmpG subunit							
WT	0.12	-	0.02	0.01	0.26	-	0.01	0.59
H200A	-	-	-	0.43	-	-	-	0.23
H202A	-	-	0.04	-	0.04	-	-	-
H203A	0.02	-	-	-	0.46	-	-	0.47
H202AH203A	-	-	-	-	0.15	-	-	0.03

Table 6: ICP-MS results determining metal content for DmpFG WT and variants. Molar equivalents of metal are based on a DmpG concentration of 0.93 μM. Metal content was tested for Mn, Co, Mg, Cu, Fe, Cd, Ni, and Fe; only metal content >0.01 eq are reported here. Content is based on comparison with standard curves.

Denaturation studies to probe the structural stability of DmpFG

A relevant question is whether or not the tightly bound metal ion identified by crystallographic analysis is required for structural stability of the DmpFG complex. If metal ion binding is mediated by His200 and/or His202, then replacing either of these residues with alanine may result in weakened affinity for the metal ion. ICP-MS results have indicated differences in metal content of the enzymes, as WT > H200A > H202A for the presence of metal (see Table 6). Any compromised structural integrity that results from less metal being bound can potentially be detected by means of protein unfolding studies with chemical or thermal denaturants. The effects of added metal ion on stability may provide additional insight.

Temperature-induced denaturation of DmpFG

Thermal denaturation of DmpFG (WT) was briefly explored. Preliminary experiments revealed that DmpFG was prone to forming insoluble aggregates at increased temperature. DmpFG samples incubated for 1 hour at room temperature, 54 and 80°C were examined by SDS-PAGE for the presence of precipitate (Figure 17). At room temperature, virtually no precipitate was formed (Figure 17, Lanes 3 & 4). At 54°C, some precipitation of both DmpF and DmpG subunits was detected (Figure 17, Lanes 5 & 6), yet a significant amount of both subunits also remained soluble. At 80°C, all protein was precipitated (Lanes 7 & 8).

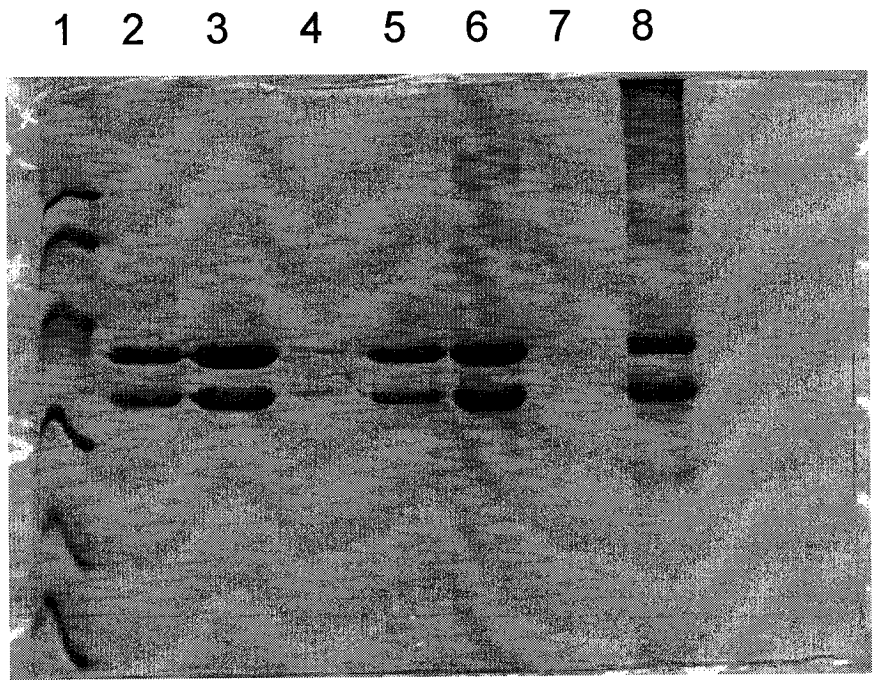

Figure 17: SDS-PAGE gel (12%) analysis of DmpFG solubility at various temperatures. Protein samples (1 mg/ml) in 50 mM HEPES, pH 8.0, were incubated at room temperature, 54 and 80°C for 1 hr., then centrifuged and for 15 min. Supernatants were removed and mixed with of 2X sample buffer, and pellets were resolubilized with an equal volume of water and 2X sample buffer. The samples were then boiled for 3-5 minutes before applying to the SDS-PAGE. Lane 1: Low molecular weight standards, 94 kDa, 67 kDa, 43 kDa, 30 kDa, 20.1 kDa and 14.4 kDa. Lane 2: DmpFG control, 5 μg. Lane 3: supernatant, room temperature. Lane 4: pellet, room temperature. Lane 5: supernatant, 54°C. Lane 6: pellet, 54°C. Lane 7: supernatant, 80°C. Lane 8: pellet, 80°C. Note that bands seen in lane 4 are not likely representative of precipitate, but rather the small amount of soluble protein that remained when the supernatant was removed.

Gd·HCl-induced denaturation of DmpFG

The use of guanidine·HCl a potential denaturant of DmpFG was explored. After several preliminary experiments it became evident that insoluble aggregates of DmpFG formed at low Gd·HCl concentrations. Figure 18 shows an SDS-PAGE gel of resolubilized DmpFG WT protein that had been precipitated with Gd·HCl. At about 0.8 M Gd·HCl, maximal precipitation was detected; the precipitate contained high levels of both DmpF and DmpG subunits (Figure 18, Lane 4). At either 0.4 or 1.2 M Gd·HCl, DmpG appeared to preferentially be precipitated over DmpF (Figure 18, Lanes 3 & 5). At higher concentrations of Gd·HCl, however, DmpFG remained soluble (Figure 18, Lane 6). Precipitation of protein at low concentrations of Gd·HCl is a characteristic of proteins that are soluble and most active under acidic conditions, such as papain (49), although DmpFG is most active in more basic solutions (11).

Similar to experiments reported using papain (49), the addition of urea was able to provide a certain measure of protection against Gd·HCl induced precipitation. When 1 M urea was added along with 0.8 M Gd·HCl to preparations of DmpFG, much less precipitate was formed (compare Figure 18 Lane 7 with Lane 4). One major cause for protein precipitation induced by Gd·HCl is the ionic nature of the denaturant. Guanidine is a positively charged denaturant, whereas urea is uncharged. A monomer of DmpG has two exposed subunit interfaces, and thus plenty of hydrophobic contacts that can lead to aggregation in the presence of charged guanidine. Precipitation can be alleviated with the more neutral urea, or by harsh conditions such as higher concentration of Gd·HCl.

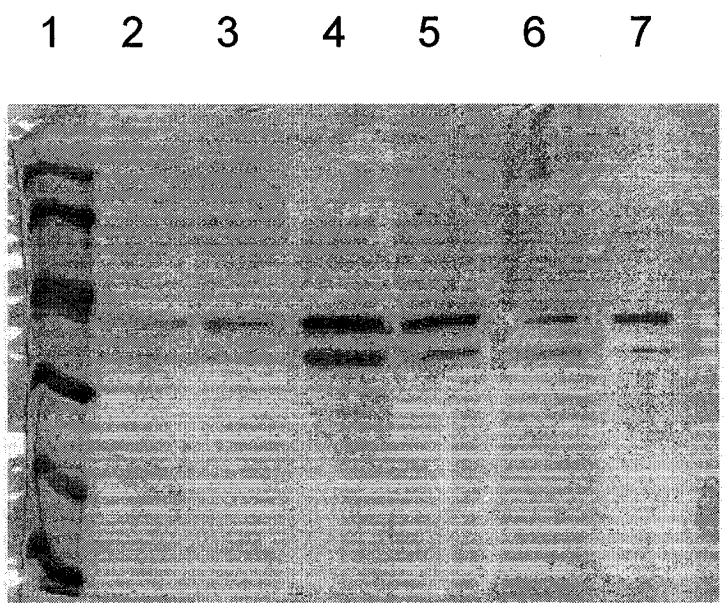

Figure 18: SDS-PAGE gel (12%) of DmpFG WT precipitated in different concentrations of Gd·HCl. Protein (0.5 mg/ml) was incubated in varying concentrations of Gd·HCl and 50 mM HEPES, pH 8.0 for 30 min. Supernatants were removed after brief centrifugation, and pellets were solubilized with 10 µl of 2X sample buffer and boiled for 3-5 minutes before applying to SDS-PAGE. Lane 1: Low molecular weight standards, 94 kDa, 67 kDa, 43 kDa, 30 kDa, 20.1 kDa and 14.4 kDa. Lane 2: precipitate from no Gd·HCl. Lane 3: precipitate from 0.4 M Gd·HCl. Lane 4: precipitate from 0.8 M Gd·HCl. Lane 5: precipitate from 1.2 M Gd·HCl. Lane 6: precipitate from 2.0 M Gd·HCl. Lane 7: precipitate from 0.8 M Gd·HCl and 1 M urea.

Aggregation of DmpFG by increased temperature or by Gd·HCl precluded any meaningful analysis of the denaturation process using these denaturants.

Urea denaturation of DmpFG WT, H200A and H202A monitored by far-UV CD

Samples of DmpFG WT, H200A or H202A were incubated in buffers containing increasing concentrations of urea, and subjected to CD scans in the far-UV region. The decrease in α-helical content of the enzymes was by monitored by the signal at 222 nm. Figure 19 demonstrates the stability profile of the enzymes: WT > H200A > H202A with $[Urea]_{50\ \%\ folded\ of}$ 3 M, 2 M and 0.5 M respectively. Only results illustrating the effects up to 5 M urea are shown, since experiments on WT demonstrated that there is no further decrease in α-helical content up to 8 M urea (data not shown).

The effects of added $MnCl_2$ on urea-mediated denaturation of WT, H200A and H202A are shown in Figure 20. A significant level of protection against urea-mediated unfolding of DmpFG H202A was observed with the addition of 1 mM $MnCl_2$ to the samples (Figure 20C), shifting the $[Urea]_{50\ \%\ folded}$ from 0.5 to about 2 M. The unfolding process does not appear to conform to a 2-state transition, and thus it is difficult to ascertain exact $[Urea]_{50\ \%}$ folded values. By comparison, there was no relative difference in the unfolding profiles of DmpFG WT or H200A when $MnCl_2$ was added (Figure 20A & B).

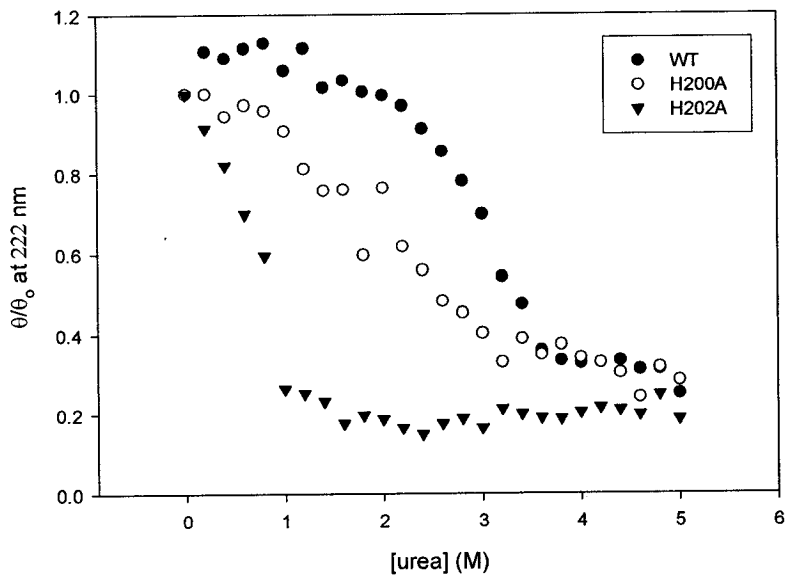

Figure 19: Urea-mediated denaturation of DmpFG WT and variants, H200A, H202A monitored by far-UV CD. Protein concentration was 0.2 mg/ml in 50 mM HEPES, pH 8.0; samples were scanned in a cell of 1 mm pathlength.

A

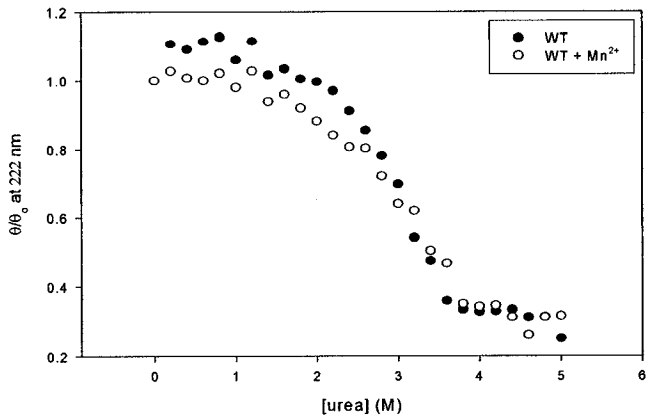

B

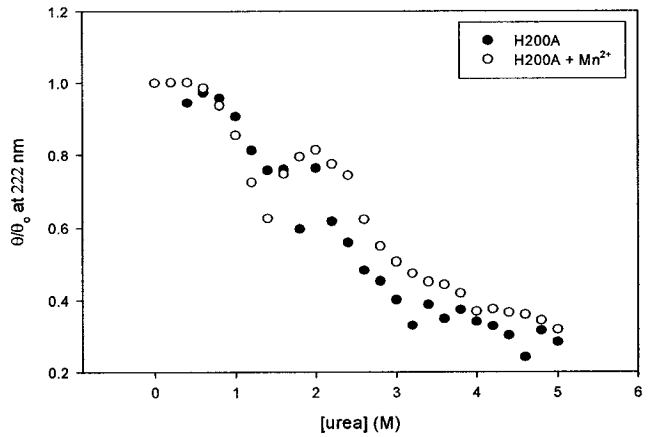

C

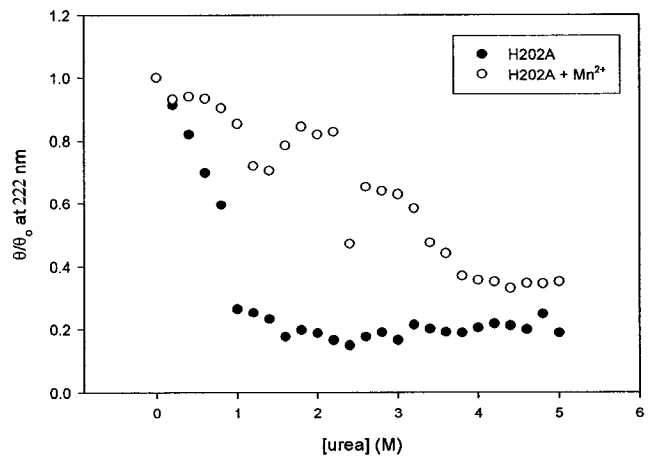

Figure 20: Urea denaturation of DmpFG A) WT and variants, B) H200A C) H202A; in the presence and absence of added 1 mM $MnCl_2$ monitored by far-UV CD. Protein concentration was 0.2 mg/ml in 50 mM HEPES, pH 8.0; samples were scanned in a cell of 1 mm pathlength.

Urea unfolding of DmpFG monitored by fluorescence

Fluorescence emission spectroscopy was used to examine the stability of DmpFG WT in the presence of urea, in terms of changes in tertiary and quarternary structure. Tryptophan fluorescence has the potential to yield information about subunit dissociation, because of the location of the lone Trp251 at the subunit interface between the two DmpG subunits. Local tertiary structure perturbations as a process of unfolding can change the environment of the tryptophan (i.e.: from non-polar to polar), and resulting changes in intensity and λ_{max} of emission spectra can be monitored.

The urea-mediated unfolding of the protein was followed by monitoring the fluorescence of samples after excitation at either 280 or 295 nm. When excited at 280 nm, distinct changes in the shape of the emission spectrum were observed as the urea concentration increased and the emission intensity decreased (Figure 21A). Samples excited at 295 nm showed a distinct shift in the tryptophan fluorescence emission, with λ_{max} increasing from 332 nm to 349 nm as the urea concentration was increased from 0 to 4.5 M urea, and the intensity decreased (Figure 21B).

The urea denaturation profiles of DmpFG WT obtained by monitoring fluorescence (tertiary structure) or far-UV CD spectroscopy (secondary structure) appear to be in good agreement to indicate that the protein is probably completely unfolded by 3.5-4.0 M urea (Figure 22). To relate relative secondary and tertiary structures of protein in various

A

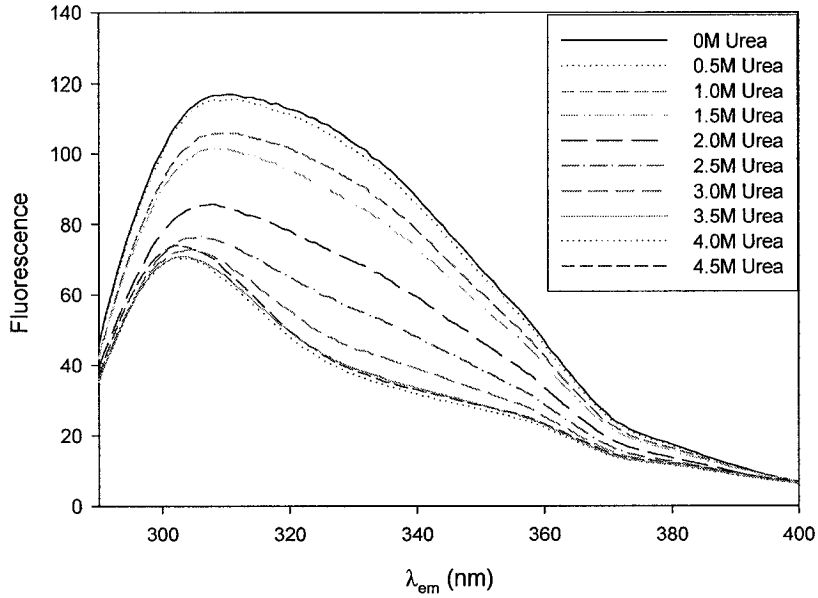

B

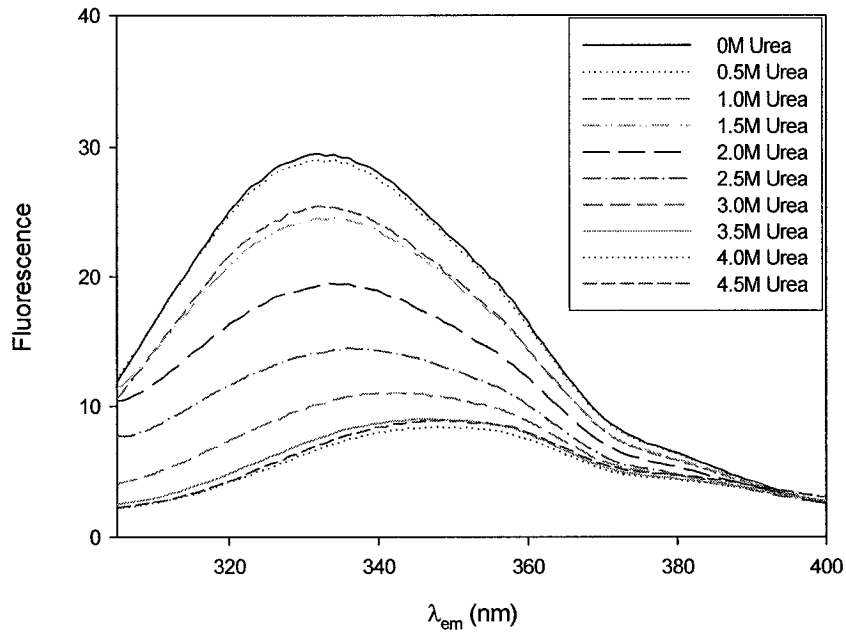

Figure 21: Urea denaturation of DmpFG WT monitored by fluorescence spectroscopy. Emission spectra were recorded using excitation wavelengths of A) 280 nm and B) 295 nm. Protein concentration of samples was 0.15 mg/ml, measured in 50 mM sodium phosphate buffer, pH 7.4.

stages of unfolding, plotting the change in relative CD signal at 222 nm and change in intensity of tryptophan fluorescence emission (λ_{ex} = 295 nm) as a function of urea concentration show distinct differences. Loss in fluorescence emission intensity occurs at urea concentrations lower than required for similar losses in CD signal, indicating that a perturbation in local tertiary structure or some protein subunit dissociation, may precede unfolding events such as loss of α-helical content.

Sedimentation velocity analytical ultracentrifugation analysis of urea-unfolded DmpFG

Sedimentation velocity AUC experiments were conducted on DmpFG WT enzyme samples that had been incubated in the presence of various urea concentrations to examine the stability of DmpFG, especially the quaternary structure. This data would be useful to compare to the CD and fluorescence results. As shown in Figure 23, over the course of denaturation there were distinct differences in the sedimentation of analyte protein molecules, indicating the change in shape and dissociation of the DmpFG subunits. In the absence of urea, DmpFG WT sedimented as a single species with a coefficient of 6.0, that corresponds to the tetrameric form of the enzyme, of 140 kDa mass (11). At 1 M urea, there was a slight shift to a lower coefficient value and higher calculated mass, which agrees with the notion that there may be an induced stabilization effect by urea at this concentration; the tetramer can adopt a more compact form which sediments with a lower sedimentation coefficient. Likewise, CD data suggests an increase in α–helical content at 1 M urea (Figure 22). At 0 and 1 M urea, > 90 % of the protein was distributed as the single

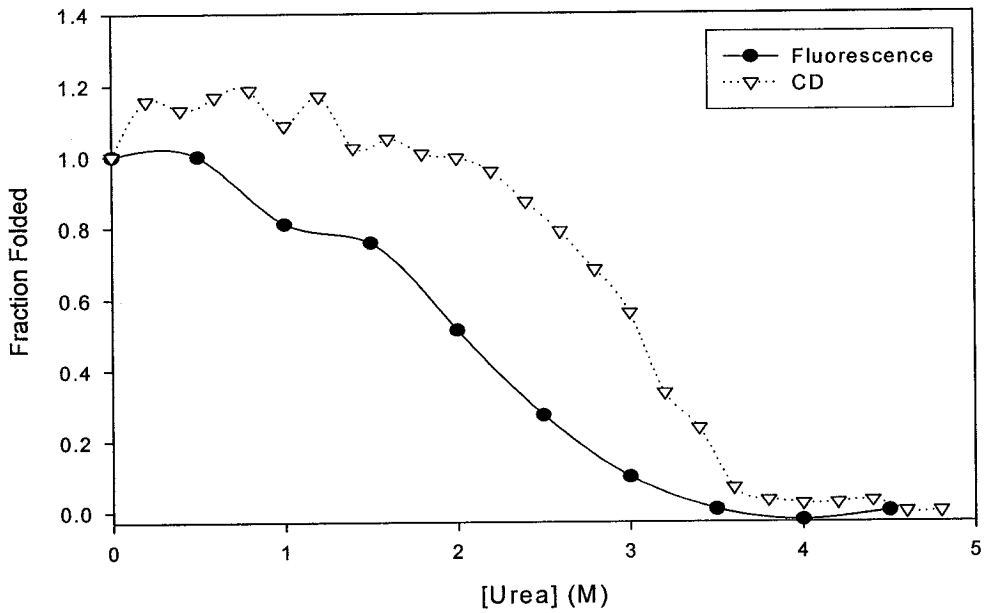

Figure 22: Comparison between far-UV CD and fluorescence spectroscopy monitoring of urea unfolded DmpFG WT. Determination of fraction folded is estimated from relative change in intensity at λ_{max} of fluorescence emission of protein excited at 295 nm, and of change in CD signal at 222 nm. Protein is taken to be 100% folded at 0 M urea, and 0 % folded at 5 M urea.

species seen in Figure 23. At 2.5 M urea there was the appearance of a major species with sedimentation coefficient of 1.8, and corresponding molecular mass 30-40 kDa, but two other types of species with higher sedimentation coefficient were also apparent. The second had an S value of about 4.2 (120 kDa) accounting for 40 % of the protein, and the third and final 40 % was broadly distributed over a wide range of S values, from 10 S to as high as 100 S. While the smallest species was likely attribute to monomers, the presence of the other two species, especially the widely distributed one, indicates that there was a large number of equilibrating species present. A concentration of 3 M urea shifted the equilibrium towards the smaller species which then accounted for about 50 % of the protein, but the broadly distributed species (10-100 S) persisted. At 4.5 M urea there was only one species which accounted for > 90% of the protein, at 1.5 S or ~ 25 kDa, demonstrative of unfolded DmpF and DmpG monomers. Corresponding CD and fluorescence data indicate that the protein is likely completely unfolded at this concentration of urea. Quite notably however, sedimentation peaks attributed to individual DmpF and DmpG monomers could not be resolved.

Transverse urea-gradient gels of DmpFG

The purpose of this experiment was to monitor the stability of DmpFG by visualizing overall changes in protein shape and oligomeric assembly as the protein migrates through a transverse urea-gradient polyacrylamide gel (45). DmpFG WT samples were applied to gels containing 0-8 M urea, and each lane had a different concentration of urea, increasing in 0.5 M increments. Gels at both pH 7.4 and 8.9 were studied (Figure 24), and the gel at pH 8.9 gave more extensive separation of bands, likely due to increased negative charge.

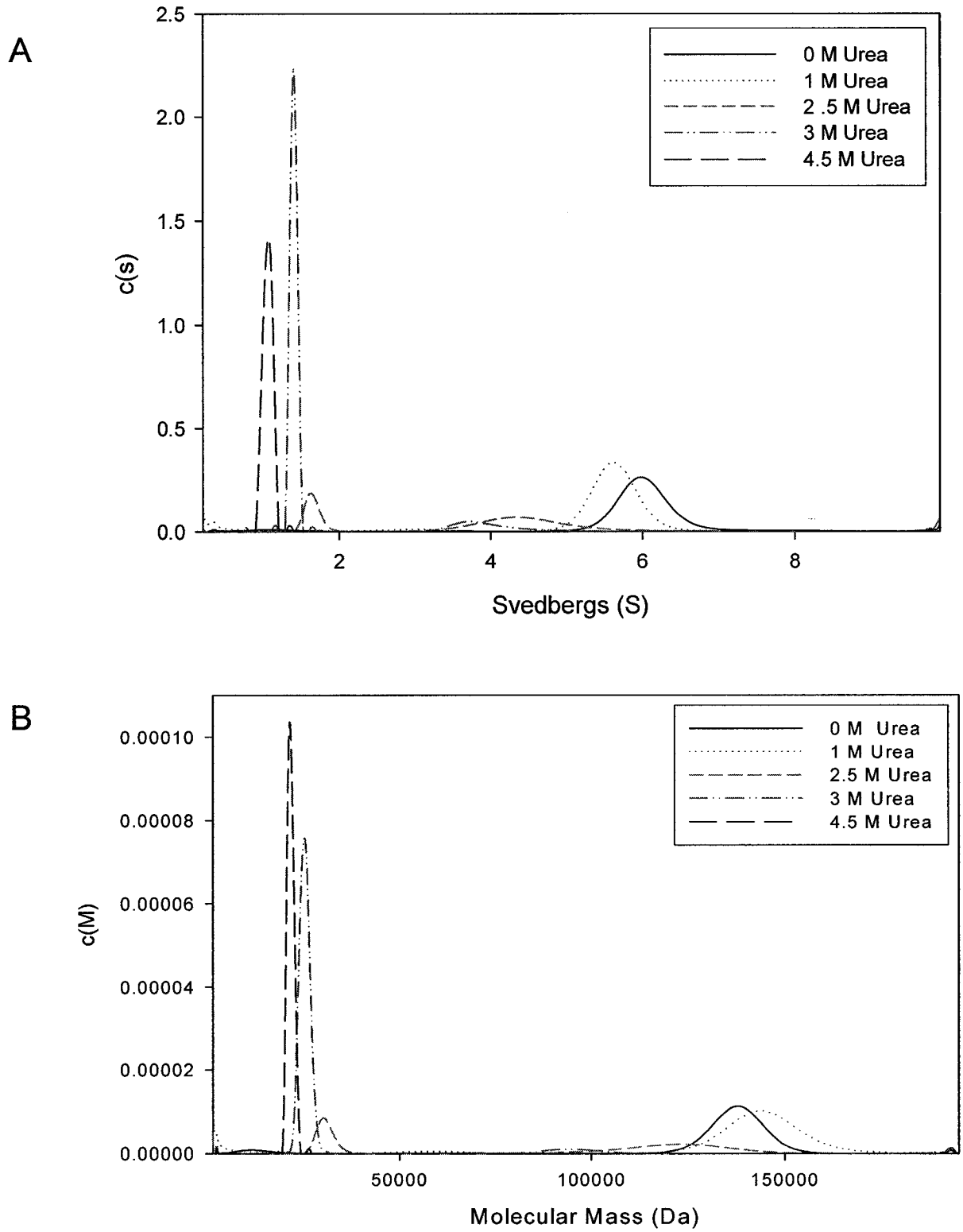

Figure 23: Sedimentation velocity AUC data for urea-denatured DmpFG WT. Data were analyzed and plot distribution was constructed using the A) c(s) model and B) c(M) model of Sedfit v8.5 software. Protein concentration was 0.5 mg/ml in 50 mM HEPES, pH 8.0; scans were collected by measuring A_{280} at 42,000 r.p.m., 20 °C.

By excising spots from the urea-gradient gels and analyzing the extracted protein by SDS-PAGE (Figure 25 and Table 7), an attempt was made to identify the locations of DmpF or DmpG subunits on the urea gradient gels. Bands were more compact in the pH 7.4 gel, and a higher proportion of DmpF and DmpG appeared to remain associated at lower urea concentration, since at similar concentrations of urea in the pH 8.9 gel only the DmpG subunit could be detected in the main band. As the subunits unfold, the protein is less mobile in moving through the gel. The unfolding transition occurs mainly between 1 and 4 M urea, consistent with CD and fluorescence data that demonstrate most of the relative secondary and tertiary structure of DmpFG is lost over the same urea concentration range. Also, as especially made evident by the gel at pH 8.9, the unfolding/dissocation processes appear complete by 4 M urea, as there is virtually no change in band display up to 8 M urea.

Although the DmpG subunit was detected, bands clearly corresponding to DmpF could not be identified at lower urea concentrations. Rather, DmpF was found diffusely, in regions near the top of the gel. At all urea concentrations, DmpF was found only in the presence of DmpG. This severely limits the ability to interpret what is going on in these experiments. However, the diffuse smeared and multiple bands at the top of the gel in response to increasing urea concentration correlates with the AUC data that suggests a large number of rapidly equilibrating species for intermediate urea concentrations.

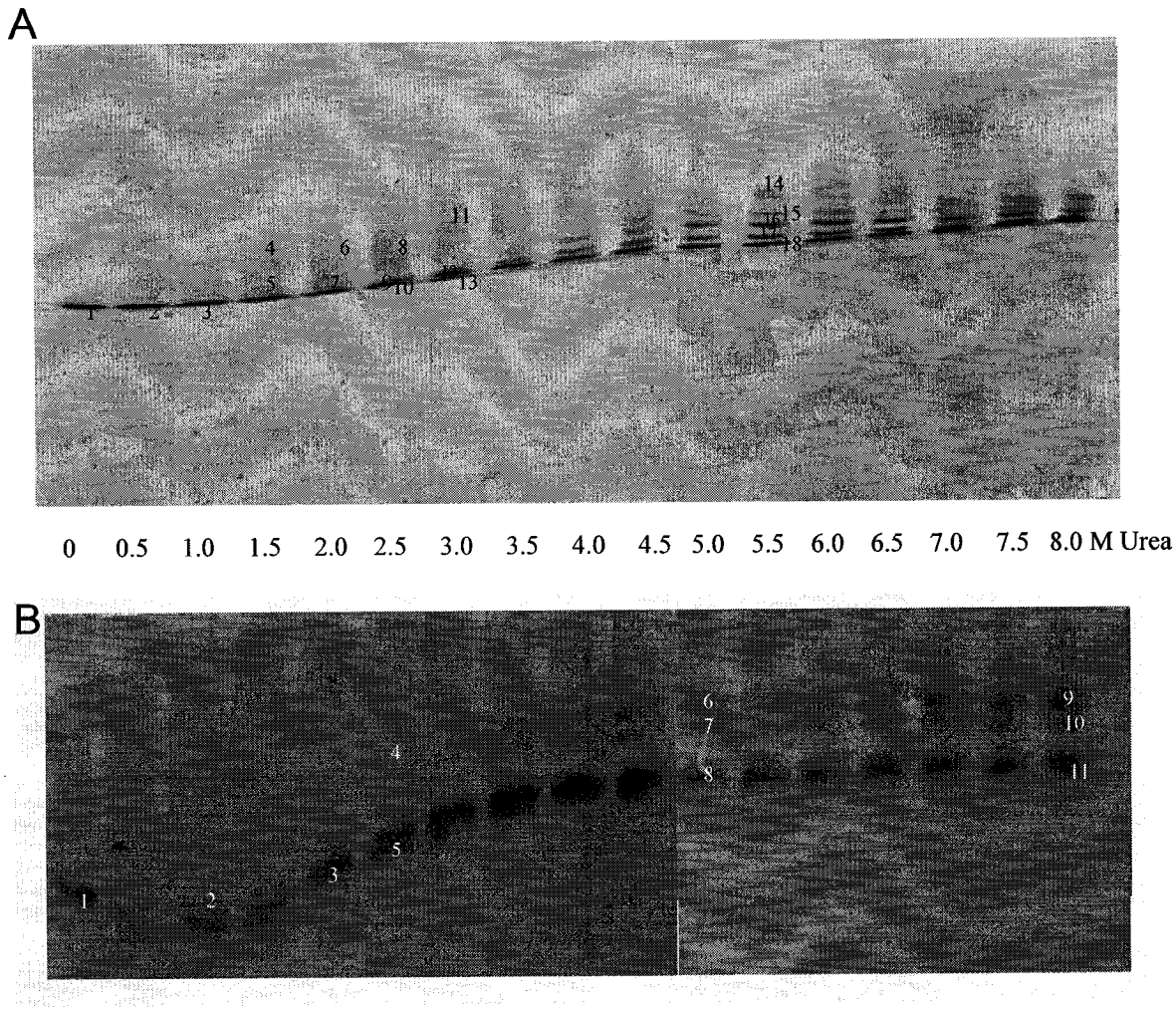

Figure 24: Tranverse urea-gradient polyacrylamide gels with DmpFG WT. Experiments were run with gels at A) pH 7.4 and B) pH 8.9. 10 μg of DmpFG enzyme was added in each lane. After the gel was run and stained with Coomassie Blue, gels spots were excised (numbered), and homogenized with SDS sample buffer. The resulting solution was then applied to SDS-PAGE and examined for the presence of DmpF (32.5 kDa) and DmpG (37.5 kDa). See Figure 25.

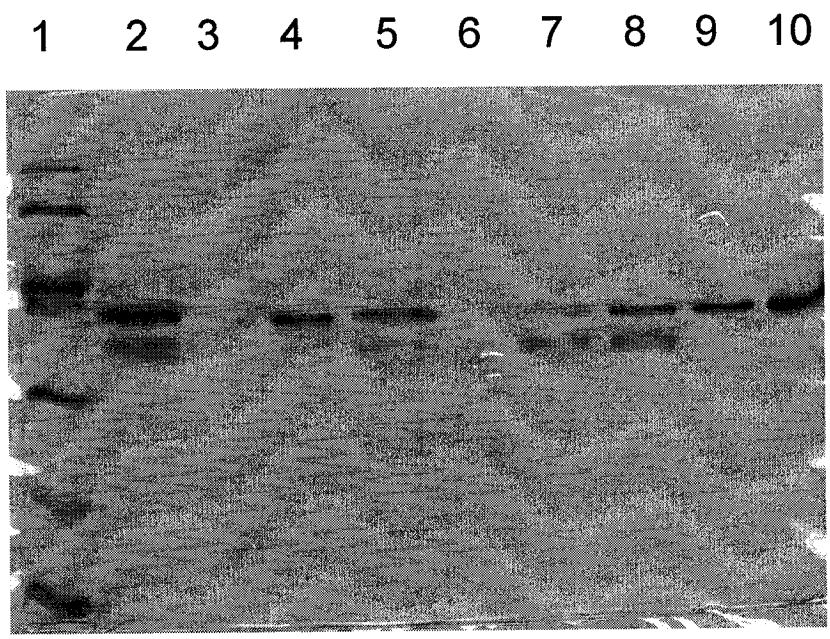

Figure 25: SDS-PAGE gel (12%) of protein extracted from urea-gradient gels. This gel is an example of those used to identify the bands numbered in Figure 24; this gel was used to identify bands #10-18 on the pH 8.9 gel seen in Figure 24B. Lane 1: Low molecular weight standards, 94 kDa, 67 kDa, 43 kDa, 30 kDa, 20.1 kDa and 14.4 kDa. Lane 2: band #10. Lane 3: band #11. Lane 4: band #12. Lane 5: band #13. Lane 6: band #14. Lane 7: band #15 Lane 8: band #16. Lane 9: band #17. Lane 10: band #18. Note that the bands of lanes 3 and 6 may be too faint to observe.

Gel at pH 7.4		Gel at pH 8.9	
Band #	Subunit(s) Detected	Band #	Subunit(s) Detected
1	F,G	1	F,G
2	G	2	F,G
3	G	3	F,G
4	F,G	4	G
5	G	5	F,G,
6	F,G	6	F,G
7	G	7	F,G
8	G	8	G
9	F,G	9	F, G
10	G	10	F,G
11	G	11	G
		12	G
		13	F,G
		14	G
		15	F,G
		16	F,G
		17	G
		18	G

Table 7: Identification of bands excised from urea-gradient gels. Excised gel fragment were analyzed for presence of DmpF and DmpG by SDS-PAGE as described. Band numbers refers to those shown in Figure 24.

Urea denaturation experiments (AUC, fluorescence, urea-gradient gels) to probe tertiary and quaternary structure of the variants were not conducted due to the complexity of results obtained with DmpFG WT.

DISCUSSION

The main objective of this thesis was to examine the catalytic and structural roles of DmpG residues His200 and His202 in the DmpFG enzyme complex. A structure obtained by x-ray crystallography showed these residues complexed with a metal ion, which in turn was complexed with a substrate analogue (15). Work done on a functionally similar enzyme, HMG-CoA lyase, demonstrated that conserved residues His233 and His235, homologous to the His200 and His202 of DmpG, were important for efficient catalysis (31, 32). In the course of this work, a third histidine residue, H203, which is conserved in DmpG, was also targeted for structure-function studies.

Purification of recombinant DmpFG WT and variants H200A, H202A, H203A and H202AH203A gave reasonably high yields of enzyme. The behaviour of the variants during purification was similar to WT, and protein yields ranged from ~17 mg (WT) to 24 mg (H202AH203A). With such changes as the use of fresh NAD^+-affinity resin and a switch from *E. coli* expression strain BL21(DE3) to C41(DE3), the yields of protein reported in this thesis are the highest obtained thus far. The protein obtained was very pure in most cases, although a persistent impurity in the H200A preparation had to be removed with an additional chromatographic step. Fortunately, the differences in DmpG structure that might result from the amino acid substitutions did not appear to grossly affect the binding of NAD^+; all variants remained tightly bound to the resin until eluted with NAD^+-containing buffer. Another concern was the solubility of the H203A and H202AH203A variants, since His203 is at the interface between the DmpG subunits (13) and mutations at this position could have potentially destabilized the protein and cause aggregation and/or

precipitation, as well as formation of inclusion bodies. Since yields similar to WT were obtained for these variants, this was not a significant problem for purification.

Biophysical characterization revealed very similar secondary and quaternary structures for all of the enzymes. Far-UV CD indicated that WT and all variants had almost identical secondary structure content. AUC sedimentation velocity experiments indicated that the WT and variants were all mainly tetrameric. There were slight differences in the AUC sedimentation profiles of the variants, especially for H203A and H202AH203A that have the H203A mutation at the DmpG subunit interface. The mutation may have slightly destabilized the quaternary structure, since there was a higher degree of subunit dissociation, as indicated by a smaller species present in the sedimentation profile. Since secondary peaks were also present in the metal-ligand variants where bound metal was absent (i.e.: H202A), it is possible that the putative metal-binding residues may also be involved in stabilizing the quarternary structure. Consistent with this notion, the double-mutant, H202AH203A, which has both an altered metal ligand and intersubunit contact, showed the highest proportion of the dissociated species. SDS-PAGE gels of the variants indicate that the smaller species is not merely a contaminating protein present in some preparations but not others.

The ICP-MS results reported in this study showed that relatively high amounts of zinc and iron and a lesser amount of manganese (0.26, 0.59 and 0.12 eq. per DmpG, respectively) were present in WT enzyme, whereas previously only manganese was found to be the most abundant metal (11). One explanation for variations in metal content could be the change

in expression host from *E. coli* strain BL21(DE3) to strain C41(DE3), which may have in different intracellular concentrations of metals. Although intracellular metal concentrations of the BL21(DE3) strain have been reported (50), there is no comparable information for the C41(DE3) strain (Personal communication, J. Walker).

Fluorescence emission spectroscopy showed that the tertiary structures of the WT and variants were significantly different. The most likely possibility is that the mutations themselves may perturb the tertiary structure, especially the microenvironment surrounding the lone tryptophan of DmpG, Trp251. The fluorescence of WT and the H203A variant were the most similar, although one might expect that the fluorescence would more different if the dissociation that was seen by AUC caused a change in the tryptophan's environment. Speculation suggests that the fluorescence differences may reflect the amounts of metal bound to each of the various enzymes if the metal ion induces tertiary structure changes. Metal analysis by ICP-MS showed that WT and H203A had ~ 1 eq. of metal bound per DmpG subunit, and the spectra of these two enzyme forms had the most similar fluorescence intensities. The fluorescence spectrum of the H202A variant, which had virtually no bound metal, was approximately 1.5-fold greater in emission intensity than WT. The metal content of H202AH203A was a little higher than H202A (0.18 and 0.08 eq. per DmpG, respectively), and the emission intensity was slightly less than H202A, but still higher than WT. The fluorescence spectrum of the H200A variant had a slight red-shift in emission wavelength, which was different than observed for the other enzymes. It is possible that a significant amount of bound copper (0.43 eq. per DmpG), which was detected only in the H200A variant, may have caused the unique λ_{max} emission shift. A

possible explanation for the fluorescence emission differences is that the tertiary structure is affected by the nature of the metal bound. For example, for phenol hydroxylase from *Pseudomonas* sp. strain CF600, apo-enzyme exhibited higher emission intensity compared to holo-enzyme that had bound Fe^{2+} (51). However, preliminary results indicated that the fluorescence emission spectra of WT, H200A, and H202A were unchanged by the presence or absence of Mn^{2+}.

DmpF dehydrogenase specific activity of the variants seemed to be consistently higher than WT, with as much as a 2-fold increase in the H202A variant. Because the K_M for acetaldehyde in WT is greater than 50 mM and only about 20 mM acetaldehyde was added to the dehydrogenase assays, it is possible that small changes in the variant K_M for acetaldehyde may have resulted in the changes in specific activity observed under the assay conditions used. Steady-state kinetics analysis of the dehydrogenase activities of the variants would shed additional light on the nature of these activity differences.

Aldolase activity was detected for WT and all variants, and was metal ion dependent. Only WT and the H203A variant had detectable aldolase activity in the absence of added metal ion, which could be stimulated several fold by the addition of metal ion to activity assays. ICP-MS analysis showed that only these two enzyme forms had any significant amount of metal ion bound, which may account for the residual activity. The metal-ligand deficient variants, H200A, H202A and H202AH203A, which had much less metal ion bound than either WT or H203A, were not detectably active unless metal ion was added to the assay mixture.

Because of His200 and His202's proposed involvement in metal ion binding, the metal requirements for WT and variant aldolase activities were examined. Differences in K_M for metal-ion would be useful in determining if His200 or His202 are involved in binding metal ion for activity, and perhaps confirming that the metal ion seen bound in the x-ray structure plays a catalytic role. The biphasic nature of metal ion dependence had both Co^{2+} and Mn^{2+} apparently saturating at a concentration of 1mM (1st phase) then an increase of activity was observed at higher concentrations (2nd phase). A concentration of 10 mM did not appear to saturate in the cases of WT, H200A (active with Co^{2+} only) and H203A. Qualitative observation did reveal that there is no notable preference by WT or H203A for either Mn^{2+} or Co^{2+}, but all of the other variants showed higher activity with Co^{2+} than Mn^{2+}. Mn^{2+} or Co^{2+} at a concentration around 5 to 10 mM actually had a slight inhibitory effect on the H202A and H202AH203A variants. The K_M for activator metals of DmpG could not be easily determined, since activity did not follow Michaelis-Menten kinetics. These results may further be interpreted in light of a previous observation, that perhaps various types of tightly bound metals interfere with activity. H202A and H202AH203, which have the least amount of metal ion bound, exhibited the highest stimulated specific activity when metal ions were added. WT, H200A and H203A all have other metals bound which may need to be displaced by high concentrations of either Co^{2+} or Mn^{2+} to achieve maximal levels of aldolase activity.

The discovery of Co^{2+} as an activator of aldolase activity was useful for the further characterization of WT and variants. Co^{2+} could stimulate the WT and variants the same

as, or to a higher degree, than Mn^{2+}, which was previously reported to be the only activating metal ion for WT (11). Despite H200A's lack of activity with Mn^{2+}, Co^{2+} was able to restore aldolase activity to this variant. It may be the subtle difference such as size or electronic configuration of the ion that make metal-ligand variants of DmpG more selective for Co^{2+} over Mn^{2+}. While it is possible that Co^{2+} is simply a better activator of DmpG aldolase activity in the metal-ligand variants, it is also possible that Co^{2+} may be more efficient than Mn^{2+} at displacing any inhibitory metals that are bound to the enzyme. Zn^{2+} inhibits DmpG aldolase activity (11), and ICP-MS results revealed the Zn^{2+} was bound in significant amounts to WT and the H203A variant (0.26 and 0.46 eq. per DmpG, respectively). The Cu^{2+} bound to H200A (0.43 eq per DmpG) may also be inhibitory. As an example, Cu^{2+} was found to be a potent inhibitor of fructose-1,6-bisphosphate class II aldolase from *T. aquaticus* (52).

Since H200 and H202 were both observed to be metal ion ligands in the crystal structure, a perplexing result was that the H202A variant exhibited a high level of aldolase activity, whereas H200A did not. Potentially, His203, a histidine residue conserved in all known 4-hydroxy-2-ketovalerate aldolases, could substitute for His202. However, since H203A and H202AH203A were found to be quite active, the possibility of His203 taking over in the absence of His202 was ruled out.

Steady state kinetics analysis of the WT and variant aldolase activities demonstrated distinct differences in apparent k_{cat} and K_M for the substrate, 4H2KV. While the WT was the most catalytically efficient (highest k_{cat}/K_M ratio) the variants were not much less

efficient. However, H200A was only active with Mn^{2+}, rather than both Mn^{2+} and Co^{2+} as were the other enzymes. The k_{cat} of the variants was largely unchanged, and appears to have been increased in some cases, especially for H202A. The K_M for 4H2KV had substantially increased several-fold for all variants, except H203A. Since His203 is positioned at the subunit interface (15), rather than the active site, it is perhaps not surprising that the K_M of this variant was unaffected. However, this mutation may still have caused a slight perturbation in tertiary structure since an approximate 4-fold decrease in k_{cat} that was observed. It may actually be tertiary structure perturbations of the variants, as detected by changes in fluorescence emission spectra, that affect K_M and k_{cat}, and not the specific residues themselves.

Comparing kinetic data obtained by coupled DmpG-LDH and coupled DmpFG assays, we observe a similar trends in the data, with the exception of the H202A variant. For WT enzyme, the DmpFG coupled reaction had about a four-fold higher turnover than that of DmpG-LDH, which may be explained by pyruvate product release being a rate limiting factor (suggested in (14)). The apparent k_{cat} of H202A was actually 3-fold lower when using the DmpFG coupled assays to measure activity. Another striking difference between the two assays was the K_M measurement for H202A. Although the apparent K_M for 4H2KV measured for the other variants remained for the most part unchanged, the K_M for 4H2KV estimated by the DmpFG coupled assays for H202A was about 7 fold lower than was estimated by the DmpG-LDH coupled assays. The significance of these differences remains to be explained.

The effects of oxalate on DmpG aldolase activity were briefly investigated, since oxalate was potentially the bound ligand observed in the structure of DmpG (15). MphE (2-hydroxypent-2,4-dienoate hydratase) from *E. coli,* which has a 40 % identity with DmpE (Figure 1) from *Pseudomonas sp.* strain CF600, produces 4H2KV and is competitively inhibited by oxalate (K_i = 4.9 +/- 0.7 μM) (53). Oxalate represents a unique transition-state analogue because of its resemblance to 4H2KV where oxalate has a negatively charged oxygen atom; there is a carbanion in the proposed enolate reaction intermediate. It also bears structural resemblance to the pyruvate product, which has a methyl group in place of an oxalate oxygen. Oxalate was found to be strongly inhibitory in WT and H203A activity assays, but much less for the other variants. The nature of inhibition has not yet been characterized, but based on the structural similarities between oxalate and pyruvate or 4H2KV, competitive inhibition is likely. Further tests are required to confirm this assumption, and to estimate K_i values. The trend of increasing K_M values for 4H2KV in the variants may correlate to the elevated $IC50_{oxalate}$ values that were observed. Although oxalate is a good chelator, it is unlikely that oxalate is simply sequestering stimulatory metal ions in the case of WT, H202A, H203A, and H202AH203A because metal ion concentration in the assay is far in excess of the oxalate concentrations required for significant inhibition. H200A is potentially the most interesting with an elevated $IC50_{oxalate}$ value of over 400 μM (compared to WT at ~ 5 μM) It is possible that oxalate in this instance is chelating the free Co^{2+}, or that Co^{2+} is poorer than Mn^{2+} at forming an inhibitory E*M*I complex, but further investigation is necessary.

Although it became apparent that neither His200 nor His202 were absolutely essential for efficient aldolase catalysis, contributions of these residues to structural stability were also examined. Using WT enzyme as a starting point for denaturation studies, thermal-, Gd·HCl- and urea-mediated protein unfolding experiments were carried out. Application of either heat or Gd·HCl presented problems because they precipitated the protein; since precipitation was not observed in the presence of urea, further studies involved this denaturant exclusively. Both CD and fluorescence experiments indicated that DmpFG was progressively unfolded by increasing concentrations of urea. Comparison of the two types of data indicated that a decrease in fluorescence occurred before a change in the far-UV CD spectra, which indicated a loss of some tertiary structure at lower concentrations of urea than required for loss of secondary structure. AUC and PAGE under urea-denaturing conditions further probed the unfolding process, especially the disassembly of the native tetrameric protein. The main complication presented by these two techniques was the fact that many equilibrating species were observed to be present at intermediate concentrations of urea, so that a clear understanding of the quaternary structure stability was difficult to obtain. At these urea concentrations, dissociating subunits were in equilibrium with an amorphous polymerization of the protein, as was evident from protein smearing on urea-denaturing gels and the AUC sedimentation peaks distributed over a wide range of large S-values. Polymerization is likely a reversible process, since solid precipitate was not observed in AUC sample solutions. At 4.5 M urea, polymerization was not observed by AUC, and the protein was dissociated into monomers. This observation of polymerization is similar to the AUC sedimentation velocity results obtained for pigeon liver malic enzyme, where polymerization of the protein occurred at concentrations of urea that caused

an intermediate amount of unfolding (54). Like DmpG, polymerization of the malic enzyme disappears at higher concentrations of urea, as the protein sediments as unfolded monomers.

A comparison of urea-mediated denaturation of WT, H200A, and H202A monitored by CD spectroscopy showed that WT > H200A> H202A in terms of stability. The relative stability of secondary structure appeared to correspond to the amount of metal bound to the enzyme, as WT has the most metal bound (~1 eq. per DmpG) and highest stability, and H202A had the least metal bound (~0.08 eq. per DmpG) and has the lowest stability. Likewise, H200A's intermediate amount of bound metal (0.66 eq. per DmpG) corresponded to intermediate stability. Added Mn^{2+} did not affect the denaturation profile of WT or H200A, but Mn^{2+} did protect against the denaturation of H202A, restoring a level of stability similar to WT. Furthermore, not only was H200A unable to use Mn^{2+} for activity, but Mn^{2+} was not able to restore secondary structure stability. An example of the use of Mn^{2+} to stabilize protein structure was also described with the alpha-1 domain of integrin I, where the addition of Mn^{2+} helped protect against urea-mediated denaturation (55) indicated by increased the $[Urea]_{50\% \text{ folded}}$ in the presence of added Mn^{2+}. The effects that added Co^{2+} has on DmpFG stability have not been examined, but future experiments may yield interesting results; it should be noted however that no significant amounts of Co^{2+} were detected in any of our samples by ICP-MS.

Human HMG-CoA lyase is potentially the most useful enzyme with which to compare the results we obtained with DmpG. Extensive site directed mutagenesis work had been previously carried out in order to examine the functional importance of His233 and His235

residues which are homologous to DmpG's His200 and His202 residues. The HMG-CoA lyase mutagenesis studies were done and interpreted without having a crystal structure. Compared to WT, variants H233A and H235 of HMG-CoA lyase had k_{cat} values that were diminished by ~6000- and 15-fold respectively; the K_M's for Mn^{2+} and HMG-CoA substrate were increased ~ 4- and 75- fold respectively for H235A, and no significant change was observed for the H233A variant. His233 was shown to be very important for catalysis, but only His235 was implicated in activator metal ion binding (31, 32). Conversely with DmpG, we observed no significant change in k_{cat} for the H200A and H202A variants, but increases in the K_M for 4H2KV substrate were observed in both variants (more than 10 fold in each case). Although no K_M values were calculated for metal ions for the DmpG WT and variants, qualitative observation revealed that H200A could not use Mn^{2+} for activity. HMG-CoA lyase variant H233A's K_M for Mn^{2+} was virtually unaltered, yet specific activity was severely reduced compared to WT. The H235A had an increased K_M, and ESR studies showed that K_D for Mn^{2+} binding had similarly increased as well. WT could bind Mn^{2+} in the absence of substrate, but added HMG-CoA was needed for detectable metal ion binding in H235A; it was suggested that the substrate itself provided the ligands necessary to bind Mn^{2+} in an E*M*S complex (32). Both Co^{2+} and Mn^{2+} are paramagnetic, so ESR should be a useful tool in examining the binding characteristics of each these activator metals ions to DmpG WT and variants.

There is the possibility that there may be two divalent ion binding sites in DmpG, one for catalytic function and another for structural stability. α-IPM synthase and HMG-CoA lyase, which have both been compared to DmpG on the basis of structural and catalytic

similarities, are shown to have more than one metal ion bound under certain conditions Despite only one metal being observed in the x-ray structure of α-IPM synthase from *M. tuberculosis*, the α-IPM synthase of *S. cerevisiae* (47 % identity) has two binding sites for Zn^{2+}, a high affinity and low affinity site (56). Systematic removal of one or both these zinc ions by dialysis with different concentrations of chelators diminished activity, and interestingly, affected the K_M for the substrates.

Narasimhan *et. al.* (57) found variable amounts of tightly-bound Cu^{2+} in HMG-CoA lyase from *P. mevalonii* (49 % identity with *H. sapiens*), whose EPR signal suggested that nitrogens, likely from histidines, are ligands to the copper (58). The most probable candidates are His204 and His206 (His233 and His235 in the human enzyme), in concurrence with the common metalloenzyme HXH metal binding motif (59). The amount of detected copper (0.07-0.7 atoms per subunit) correlates with thermostability, as having more copper bound prevented substantial loss of activity at 30°C (57). As was observed in the urea denaturation studies of DmpFG WT and variants, the increased amount of bound metal correlated with increased stability. Varying copper content, however, did not affect the affinity of HMG-CoA lyase for dissociable activator cations, Mn^{2+} or Mg^{2+} (57). For the sake of comparison, the human HMG-CoA lyase unfortunately has not been surveyed for other metals (H. Miziorko, personal communication), so it is unknown if there is tightly bound copper present, and what effects mutations have on the potential binding of a structurally required metal.

Class II fructose-1,6-bisphosphate aldolases from *E. coli* or *T. aquaticus* (21, 17), are examples of aldolases that have two metal ion binding sites in close proximity to each other. Discovery of two metal ions in fructose-1,6-bisphosphate aldolase from *E. coli* was a systematic process, starting with the belief that there was only one metal bound per subunit, and removal of the lone metal caused loss of activity (60). Later, when two metals were identified in the x-ray crystal structure, zinc was identified as one and the other's identity remained unknown (21) until it could be firmly established that it was indeed two zinc ions bound, side by side (61) one assigned a structural role, and the other a catalytic role .

Obtaining preparations of metal-free DmpG apoenzyme will be a very important goal for future work, so that the correlation can be made between the number and type of metal ions bound with the amount of enzyme activity and structural stability. Unfortunately, attempts to obtain apoenzyme in the past have been unfruitful, as 5 mM EDTA (11) or 50 mM 8-hydroxyquinoline-5-sulfonate (personal communication, J. Powlowski) did not abolish the residual aldolase activity of WT enzyme. A complicating factor may be the bound molecule (possibly oxalate) seen in the structure of DmpG, which may block access of the chelators to the bound metal ion. Similar difficulties in creating an apo- α-IPM synthase have been reported (56) and it was discovered that although 50 mM EDTA could remove at most 85 % of the metal bound, there was still some residual activity and metal ion present. It will be necessary to try other chelators to create metal-free DmpFG apoenzyme. On the other hand, an alternative approach may be to obtain enzyme with higher homogeneity of metal content, rather than having a mixture of bound metals, as we have observed. By

supplementing growth media with the metal ion of interest, the cation may be incorporated into the protein at time of expression. Such an observation was made with recombinant bacteriophage lambda protein phosphatase, expressed in *E. coli* in the presence of various divalent metal ions (50).

Creation of new variants of DmpG to probe other putative active-site residues is of obvious interest. The catalytically important activator metal-ligand residues Glu72, His235 and Asp42 of HMG-CoA lyase have been identified by site-directected mutagenesis, and based on a model of HMG-CoA lyase that used the structure of DmpG as a template, they align closely with Glu48, His202 and Asp18 of DmpG (24). It is possible that although His200 and His202 of DmpG were observed in the x-ray structure as metal-ligating residues, and mutations of these residues can have effects on catalytic efficiency and structural stability, they are shown in this study to be not absolutely essential for catalysis. However, if the mutations were to occur *in vivo,* limited metal ion selectivity and increased K_M for the substrate may render the organism severely hindered or non-viable under certain growth conditions (i.e. in the presence of catechol). Taking our results together with those obtained for HMG-CoA lyase, other residues in DmpG such as Glu48 and/or Asp18, may also play roles in interacting with a catalytically-required metal ion, while His200 and His202 may be more involved with binding a metal ion for structural stability. The stabilizer residues that hydrogen-bond to DmpG's His200 and His202, which are conserved in α-IPM synthase and partially conserved in HMG-CoA lyase, should also be examined for their structural and catalytic contributions. Our current structural model and site-

directed mutagenesis results suggest that metal ion binding within DmpG is a complex phenomenon, of which many amino acid residues are certainly involved.

REFERENCES

1. Lister, J. (1837) *Lancet.* (March 16) 326-329937
2. McGrew, R. E. (1985) Encyclopedia of Medical History (pp 20-34). Macmillan Reference books, MacMillan Press, London.
3. Anonymous (2000) Priority Substance List Assessment Report: Phenol. Ottawa: Environment Canada/Health Canada.
4. Deely, G.M., Skierkowski, P. Robertson, J.M. (1985) *Applied and Environmental Microbiology* 49:4 867-869.
5. Gray, P.H.H., Thornton, H.G. (1928) *Cent Bakt Parasitenk II Abt* 73:74-96.
6. Happold, F.C. Key, A. (1932) *Journal of Hygiene*. 32:573-580
7. Bayly R.C., Barbour M.G. (1984). Microbial Degradation of Organic Compounds. (pp 253-294) Ed. by Gibson, D.T. Marcel Dekker, New York.
8. Ornston, L.N., Yeh, W.K. (1982) Biodegradation and Detoxification of Environmental Pollutants (pp 105-126) Ed. by Chakrabarty, A. M. CRC Press, Boca Raton, FL.
9. Shingler, V., Franklin, F. C. H., Tsuda, M., Holroyd, D. and Bagdasarian, M. (1989) *Journal of General Mircobiology*. 135:1083-1092.
10. Powlowski, J., Shingler, V. (1994) *Biodegradation* 5: 219-236.
11. Powlowski, J., Sahlman, L., Shingler V. (1993) *J. Bacteriol.* 175(2): 337-385.
12. Shingler, V., Powlowski, J., Marklund, U. (1992) J. Bacteriol. 174(3): 711-724.
13. Manjasetty, B. A., Croteau, N., Powlowski, J., Vrielink, A. (2001) *Acta. Crystallogr. D Biol. Crystallogr.* 57(4): 582-5.
14. Monastariokas, S. (1998) M.Sc. Thesis. (Concordia University, Montreal)

15. Manjasetty, B. A., Powlowski, J., Vrielink, A. (2003) *Proc. Natl. Acad. Sci.* 100(12) 6992-6997.

16. Rutter, R. J. (1964) *Fed. Proc.* 23: 1248-1257.

17. Izard, T., Sygusch, J. (2004) *J. Biol. Chem.* 279(12): 11825-11833.

18. Dreyer, M. K., Schulz, G.E. (1993) *J. Mol. Biol.* 231: 549-553.

19. Kroemer, M., Merkel, I., Schulz, G.E. (2003) *Biochemistry* 42(36): 10560-10568.

20. Izard, T., Blackwell, N. C. (2000) *EMBO J.* 19: 3849-3856.

21. Cooper, S. J., Leonard, G. A., McSweeney, S. M., Thompson, A. W., Naismith, J. H., Qamar, S., Plater, A., Berry, A., Hunter, W. N. (1996) *Structure* 4: 1303-1315.

22. Hall, D. R., Bond, C. S., Leonard, G. A., Watt, C. I., Berry, A., Hunter, W. N. (2002) *J. Biol. Chem.* 277: 18-24.

23. Altschul, S.F., Madden, T.L., Shäffer, A.A., Zhang, J., Zhang, Z., Miller, W., Lipman, D.J. (1997) *Nucleic Acids Res.* 25: 3389-3402

24. Tunistra, R. L., Wang, C.Z., Mitchell, G. A., Miziorko, H. M. (2004) *Biochemistry* 43: 5287-5295.

25. Koon, N., Squire, J., Baker, E. N. (2004) *Proc. Natl. Acad. Sci.* 101(22): 8295-8300.

26. Kohlhaw, G.B. (1988) *Methods Enzymol.* 166: 14-423.

27. Kohlhaw, G.B., Leary, T. R., Umbarger, H. E. (1969) *J. Biol. Chem.* 244: 2218-2225.

28. Stegink, L.D., Coon, M.J. (1968) J. Biol. Chem 243: 5272-5279.

29. Roberts, J. R., Chakravarthy, N., Hruz, P.W., Mitchell, G. A., Miziorko, H. M. (1994) *J. Biol. Chem.* 269:27 17841-17846.

30. Mitchell, G. A., Ozand, P. T. Robert. M.-F., Ashmarina, L. Roberts, J., Gibson,

K.M., Wanders, R.J., Wang, S., Chevalier, I., Plchl, E., Miziorko, H. (1998) *Am. J. Hum. Gen.* 62: 295-300.

31. Roberts, J. R., Mitchell, G. A., Miziorko, H. M. (1996) *J. Biol. Chem.* 271(40): 24604- 24609.
32. Roberts, J. R., Miziorko, H. M. (1997) *Biochemistry* 36(24): 7594-7600.
33. Tunistra R. L., Miziorko, H. M. (2003) *J. Biol. Chem.* 278(39): 37092-37098.
34. Cassals, N., Gómez-Puertas, P., Pié, J., Mir, C., Roca, R., Puisac, B., Aledo, R., Clotet, J., Menao, S., Serra, D., Asins, G., Till, J., Elias-Jones, A. C., Cresto, J. C., Chamoles, N. A., Abdenur, J. E., Mayatepek, E., Besley, G., Valencia, A., Hegardt, F.G. (2003) *J. Biol. Chem.* 278:31 29016-29023.
35. Roberts, J. R., Narasimhan, C., Miziorko, H. M. (1995) *J. Biol. Chem.* 270:29 17311-17316.
36. Dawson, R., Elliot, D., Elliot, W., Jones, K. (1986) *Data for Biochemical Research, 3rd Edition.* Clarendon Press. Oxford.
37. Sambrook, J., Fritsch, E. F., and Maniatis, T. (1989) *Molecular Cloning: a Laboratory Manual,* 2nd ed., Cold Spring Harbor Laboratory Press, Cold Spring Harbor.
38. Tabor, S., Richardson, C. C. (1985) *Proc. Natl. Acad. Sci.* 82(4):1074-8.
39. Miroux, B., Walker, J. E. (1996) *J. Mol. Biol.* 260(3) 289-98.
40. Coligan, J. E., Dunn, B.M., Ploegh, H. L., Speicher, D. W., Wingfield, P.T. (2004) *Current Protocols in Protein Science.* John Wiley & Sons.
41. Tynan, J., Forde, J., McMahon, M., Mulcahy, P. (2000) *Protein Expression and Purification* 20(3): 421-434.

42. Brown, R.E., Jarvis, K. L., Hyland, K. J. (1989) *Anal Biochem.* 180(1):136-9.

43. Mach, H., Middaugh, C. R., Lewis, R.V. (1992) *Anal Biochem.* 200(1):74-80.

44. Johnson, A.E., Tanner, M.E. (1998) *Biochemistry* 37: 5746-5754

45. Gentile, F., Veneziani, B. M., Sellitto, C. (1997) *Anal. Biochem.* 244: 228-232.

46. McLellan, T. (1982*)* *Anal. Biochem.* 126:94-99.

47. Laemmli, U.K. (1970) *Nature (London)* 227:680-685.

48. Dagley, S., Gibson, D. T. (1965) *Biochem. J.* 95:466-474.

49. Edwin, F., Sharma, Y. V., Jagannadham, M. V. (2002) *Biochem. Biophys. Res. Commun.* 290(5):1441-1446.

50. Reiter, T. A., Reiter, N. J., Rusnak, F. (2002) *Biochemistry* 41: 15404-15409.

51. Cadieux, E. (2002) Ph.D. Thesis (Concordia University, Montreal)

52. Freeze, H., Brock, T.D. (1970) *J. Biol. Chem.* 101(2): 541-550.

53. Pollard, J.R., Bugg, T.D. (1998) *Eur. J. Biochem.* 251(1-2):98-106.

54. Chang, H.-C., Chou, W.-Y., G.-G. Chang (2002) *J. Biol. Chem.* 277(7) 4663-4671

55. Gotwals, P. J., Chi-Rosso, G., Ryan, S. T., Sizing, I., Zafari, M., Benjamin, C., Singh, J., Venyaminov, S. Y., Pepinski, R. B., Kotelianski, V. (1999) *Biochemistry* 38(26): 8280-8.

56. Roeder, P. R., Kohlhaw, G. B. (1980) Biochim. Biophys. Acta. 613: 482-487

57. Narasimhan, C., Miziorko, H. M. (1992) *Biochemistry* 31: 11224-11230.

58. Narasimhan, C., Antholine, W.E., Miziorko, H. M. (1994) *Arch. Biochem. Biophys.* 312(2): 267-273.

59. Vallee, B. L., Auld, D. S. (1993) *Acc. Chem Res.* 26543-551

60. Berry, A., Marshall, K. E. (1993) *FEBS* 318(1)11-16.

61. Blom, N.S., Tetreault, S., Coulombe, R., Sygusch, J. (1996) *Nat. Struct. Biol.* (10):856-62.